Assessing the Accuracy and Reliability of Root Crack and Fracture Detection in Teeth Using Sweep Imaging with Fourier Transform (SWIFT) Magnetic Resonance Imaging (MRI)

A THESIS
SUBMITTED TO THE FACULTY OF
UNIVERSITY OF MINNESOTA
BY

Tyler J. Schuurmans, DDS

IN PARTIAL FULFILLMENT OF THE REQUIREMENTS
FOR THE DEGREE OF
MASTER OF SCIENCE

Dr. Scott B. McClanahan

August 2017

Acknowledgements

I would like to express my sincere gratitude to the following people:

Dr. Nixdorf, Dr. Idiyatullin, Dr. Law, Dr. Gaalaas, Dr. Barsness, Dr. Roach,

For your assistance, guidance, and willingness to support me in the development of this research. Your constant willingness to share knowledge and expertise was greatly appreciated.

Dr. McClanahan

For your leadership and guidance throughout the last 26 months. Your residency – an evidence-based curriculum structured around the core aspects of literature, research, and academics – is exquisitely organized and equally demanding. You have set me on a path that will lead to eventual board-certification and a career full of critical analysis and life-long learning; for that, I am truly thankful.

My Co-Residents, Endodontics Faculty, and Staff

For the lasting memories and endless laughs shared in the resident room and throughout the clinic. It was a demanding two-years, but your presence made life much more carefree and enjoyable. I am thankful we crossed paths and consider myself incredibly lucky to have your friendship. Cheers!

Dedication

To my parents, for your continual love, support, and assistance in helping me become who I am today.

To my beautiful wife Alison, for your enduring strength and support throughout this life journey. You truly are a gift to my life. With a great, big smile – many thanks and much love.

To my dearest son Henny, daddy loves you. I promise my school studies are nearly over, allowing more time for us to 'play with toys', 'eat treats', and 'read more books'. Keep smiling!

Abstract

Introduction: Magnetic Resonance Imaging (MRI) has the potential to aid in determining the presence and extent of cracks/fractures in teeth due to more advantageous contrast, without ionizing radiation. An MRI technique called Sweep Imaging with Fourier Transform (SWIFT) has overcome many of the inherent difficulties of conventional MRI with detecting fast-relaxing signals from densely mineralized dental tissues. The objectives of this *in vitro* investigation were to develop MRI criteria for root crack/fracture identification in teeth and to establish intra- and inter-rater reliabilities and corresponding sensitivity and specificity values for the detection of tooth-root cracks/fractures in SWIFT MRI and limited field of view (FOV) CBCT.

Materials and Methods: MRI-based criteria for crack/fracture appearance was developed by an MRI physicist and 6 dentists, including 3 endodontists and 1 Oral and Maxillofacial (OMF) radiologist. Twenty-nine human adult teeth previously extracted following clinical diagnosis by a board-certified endodontist of a root crack/fracture were frequency-matched to 29 non-cracked controls. Crack/fracture status confirmation was performed with magnified visual inspection, transillumination and vital staining. Samples were scanned with two 3D imaging modalities: 1) SWIFT MRI (10 teeth/scan) via a custom oral radiofrequency (RF) coil and a 90cm, 4-T magnet; 2) Limited FOV CBCT (1 tooth/scan) via a Carestream (CS) 9000 (Rochester, NY). Following a training period, a blinded 4-member panel (3 endodontists, 1 OMF radiologist) evaluated the images with a proportion randomly re-tested to establish intra-rater reliability. Overall observer agreement was measured using Cohen's kappa and levels of agreement judged using the criteria of Landis and Koch. Sensitivity and specificity were computed with 95% confidence interval (CI); statistical significance was set at $\alpha \leq 0.05$.

Results: MRI-based crack/fracture criteria were defined as 1-2 sharply-delineated, high-signal (bright/white) line shape(s) that must be visible on multiple contiguous image slices. The line shape(s) must present as: single entities, or parallel pairs in close

proximity, or pairs in close proximity exhibiting convergence or divergence extending from the external boundary of the tooth to the pulpal cavity. Intra-rater reliability for MRI was fair-to-almost perfect (κ=0.38-1.00) and for CBCT was moderate-to-almost perfect (κ=0.66-1.00). Inter-rater reliability for MRI was fair (κ=0.21; 95%CI:0.10-0.31; p< 0.001) and for CBCT was moderate (κ=0.45; 95%CI:0.34-0.56; p<0.001). Sensitivity: MRI=0.59 (95% CI:0.39-0.76; p=0.46); CBCT=0.59 (95% CI:0.59-0.76; p=0.46). Specificity: MRI=0.83 (95% CI:0.64-0.94; p<0.01); CBCT=0.90 (95% CI:0.73-0.98; p<0.01).

Conclusions: Education and training for both imaging modalities is needed to improve reliabilities for the identification of tooth-root crack/fractures. Despite the advantages of increased contrast and absence of artifact from radio-dense materials in MRI, comparable measures of sensitivity and specificity (in relation to CBCT) suggest quality MRI improvements are needed, specifically in image acquisition and post-processing parameters. Given the early stage of technology development and multiple available pathways to optimize MR imaging of teeth, there may be a use for SWIFT MRI in detecting cracks and fractures in teeth.

Table of Contents

List of Tables

List of Figures

INTRODUCTION

Cracks and fractures in teeth can pose a diagnostic dilemma and if undetected can result in pulpal pathology and clinical signs and symptoms that often require surgical intervention (1). The presences of such physical discontinuities in the external tooth surface considerably shortens the time interval necessary for the usual irritants, such as saliva, bacteria, and chemical substances to reach and affect the pulp. The closer cracks are to the pulp, the poorer the prognosis (2). The presence, location, and extent of a crack or fracture is thought to have a direct influence upon tooth survival; therefore, correctly identifying whether one is present or not is needed for prognostication (3). The American Association of Endodontists (AAE) Colleagues for Excellence document (2008) states "Lack of knowledge concerning the type, characterization and variety of fractures may lead to misunderstanding with incorrect diagnosis and inappropriate treatment" (4). Further, the AAE calls for more research in this area (5), as significantly, patients need to be "fully informed" in cases where "the prognosis is questionable" due to cracks (4).

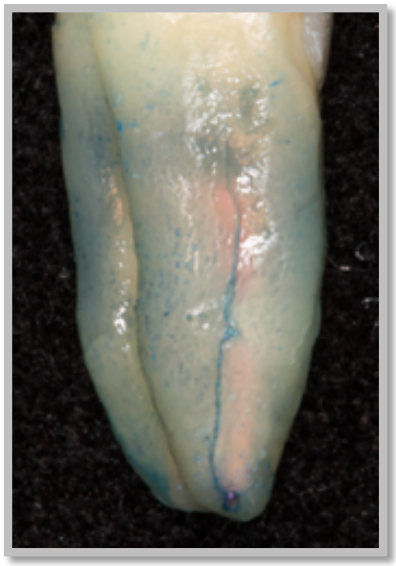

Figure 1. Example of a vertical root fracture (VRF) in a previously root canal treated, adult mandibular second molar.

Visual approaches (inspection via vital staining, magnification and transillumination) are limited in their ability to determine crack and fracture extension apical to restorations or gingival attachment (6) while definitive diagnosis can only be determined at the time of surgical exposure and direct visualization (7–9); therefore, unnecessary invasive surgical exposure and/or extraction are often completed due to lack of definitive pre-operative diagnosis (1).

Ionizing radiation-based imaging modalities, such as traditional two dimensional (2D) radiography, can aid in diagnosis but will only reveal root cracks or fractures when a fractured segment has significant displacement (10) and the X-ray beam is positioned parallel to the discontinuity (11,12). As a result, emerging three-dimensional (3D) imaging modalities, such as limited field of view (FOV) cone beam computed tomography (CBCT), have been proposed as an aid to crack and fracture detection (13). However, the results have been variable and these x-ray-based techniques require higher resolution for diagnosis, leading to an increase in both scan times and radiation dose (14). The most recent American Academy of Oral & Maxillofacial Radiology (AOMR) recommendation guidelines on CBCT use in endodontics adheres to "as low as reasonably achievable" (ALARA) principles, advocating its judicious use by clinicians who must weigh the benefit of additional diagnostic information versus the risk of ionizing radiation. Consideration must be given to the overall radiation dose over time and the increased dosages of 3D imaging over traditional 2D film and digital radiography (15).

While increased sensitivity and specificity values have been reported with limited FOV CBCT (16), detection has proven unreliable and appears dependent both on fracture width and completeness (17). A recent survey of AAE members demonstrated criticisms from respondents in regards to limitations of CBCT to include low resolution and/or the questionable diagnosis of cracks and root fractures (18). Therefore, Magnetic Resonance Imaging (MRI) may be an alternative diagnostic imaging method for determining the presence and extent of root cracks and fractures, due to more advantageous contrast, acquisition of a three-dimensional data set, inclusion of useable information about the soft tissues, and avoidance of ionizing radiation (19).

The source of a Magnetic Resonance (MR) signal in clinical scanners are the protons located in water molecules. Densely calcified enamel and dentin have relatively low amounts of water when compared to other structures within the human body, resulting in small amounts of MR signal coming from these tissues. Furthermore, the crystalline structure of these densely calcified tissues constrains the movement of water molecules, which decreases the proton relaxation time and shortens the time available to detect the MRI signal. When a tooth has a crack or fracture, a twofold effect occurs; a) more water is present in this discontinuity of tooth structure (i.e. more signal) and b) the water is less restricted within (i.e. longer time to detect signal) (19). Due to this significant increase in signal with cracks or fractures with maintenance of an acceptable contrast to noise ratio, even a narrow gap in tooth structure smaller than the size of an image voxel can cause an observable intensity contrast, a phenomenon referred to as partial volume effect (20). Thus, the voxels in the area of a crack need only gain a small amount of signal to appear bright and therefore be identified visually in the resultant image amongst a very low signal (*a.k.a.* dark) aspect of the densely calcified tissues. This characteristic, which is advantageous with MRI, is one of the limitations experienced with x-ray based imaging techniques. The contrast is low when using ionizing radiation because little relative change occurs in the mineral concentration within a cracked or fractured tooth. Consequently, when using X-ray based imaging, voxel sizes comparable with crack thickness are required to detect a tooth discontinuity, which translates to only the detection of larger cracks and fractures imaged with CBCT (11).

Given that i) the location of cracks/fractures can have a significant impact on prognosis of teeth ii) challenges remain in determining the presence of cracks/fractures in teeth with x-ray-based imaging systems, iii) avoidance of ionizing radiation is preferred in imaging tasks, iv) MRI techniques have inherent advantages in relation to x-ray based systems, and v) recent advancements in MRI technology have increased image quality at clinically relevant scan times suitable for dental applications (21,22); the objectives of this study were to develop MRI criteria for root crack/fracture identification in human teeth, measure intra- and inter-rater reliability for crack/fracture detection using SWIFT MRI and limited FOV CBCT, and to determine the sensitivity and specificity of MRI and

CBCT for the detection of tooth-root cracks/fractures when compared to known crack/fracture status.

LITERATURE REVIEW

Clinical Significance: Cracks and Fractures

Tooth fracture has been reported as the third most common cause of tooth loss after only dental caries and periodontal disease (23,24). The clinical suspicion and/or definitive diagnosis of cracks and fractures is also increasing, due in part to improved awareness of the phenomenon but perhaps most notably, people are retaining teeth longer as life expectancy has increased. As a byproduct of this rapidly increasing dentition age, a higher cumulative lifetime history of complex restorative and endodontic procedures is likely to result, pre-disposing teeth to higher crack susceptibility. Teeth will often present with one or both marginal ridges restored leading to a significantly higher prevalence of cracked tooth signs and symptoms due to loss of marginal ridge(s) (25,26).

In addition to dental procedures, between 5-25% of children and adults are estimated to have some level of destructive parafunctional habit(s) such as bruxism, causing accelerated dental attrition, especially in females and those patients of younger age (27–29). A range of epidemiologic studies have demonstrated that the majority of the population (85-90%) will have a degree of bruxism at some point in their life time (30–32) and as a destructive dental functional disorder, it can predispose a tooth to various cracks and fractures that can reduce clinical prognosis (33).

Incomplete longitudinal tooth fractures can pose a diagnostic dilemma to the clinician and if undetected can result in pulpal pathosis and clinical signs and symptoms that often require invasive surgical intervention for diagnosis and treatment. These longitudinal fractures imply a vertical component with a change over time (34), and are primarily the result of continuous occlusal forces and dental procedures rather than immediate fracture induction as in dental trauma (35) – which is not the focus of the present study. The signs, symptoms and radiographic appearance of cracks and fractures will often mimic marginal periodontal bone loss or apical periodontitis with features such

as a “halo”-type radiographic lesion or as narrow, deep periodontal probings. Arriving at a definitive diagnosis of crack and/or fracture on the basis of such signs and symptoms – limited by their highly subjective determination – can be problematic (36,37).

Discontinuities in mineralized tooth structure act as a conduit and may shorten the time interval necessary for the usual oral irritants, such as salivary components, bacteria, and chemical substances to reach and affect the vital dental pulp. Studies have demonstrated that cracks always contain bacterial biofilm colonization (38,39), presenting as a continual presence of pathogens. Technically proficient and initially successfully endodontic treatment can be liable to re-infection due to the lack of adequate seal around a crack or fracture, resulting in continual microleakage that can lead to unfavorable prognosis with possible post-operative complications (40). When the crack or fracture extends into or near the periodontal apparatus, extensive periodontal (41) and/or periapical bone loss may occur, ultimately leading to consideration of extraction as the most suitable treatment option (3).

The clinical significance regarding cracks and fractures in teeth is centered on those that enter the root but cannot be visualized in the absence of invasive measures such as initiating non-surgical endodontic access under magnification or via surgical access and visualization through incision and full-thickness muco-periosteal flap reflection, regardless of preoperative pulpal diagnosis (7,8). Root canal treatment can be considered as an important last treatment option in attempts to save cracked teeth. However, endodontic treatment is not without significant expense in terms of time and monetary costs and few studies have analyzed endodontic outcomes of cracked teeth with a near complete lack of studies with a longer term follow up (>2yrs) (42).

The location and extent of a crack may have a direct influence upon the prognosis for a given tooth; therefore possible cracks must be identified prior to dental treatment (3). Cracks that are found to progress into the pulpal chamber can significantly lower overall prognosis (43,44). The AAE Colleagues for Excellence document (2008) states “Lack of knowledge concerning the type, characterization and variety of fractures may lead to misunderstanding with incorrect diagnosis and inappropriate treatment.” Therefore, clinical dentistry is in need of a non-invasive, efficient and accurate diagnostic

method to better evaluate radicular fracture pathosis in attempts to establish a more predictable dental prognosis. If definitive crack or fracture detection could be completed earlier, at the time of initiation, existing timely interventions could be employed (45–47) or prospective techniques developed (48,49) to prevent the imminent propagation that may lead to early tooth loss. Furthermore, non-invasive and accurate early identification of cracks and fractures within teeth may mitigate the need for exploratory surgery and prevent the impending loss of supporting periodontal bone that is associated with identification further along in the pathological process.

Definition and Classification: Cracks and Fractures

The American Association of Endodontists (AAE) categorizes cracks and fractures into 5 types with regards to longitudinal orientation: craze lines, fractured cusp, cracked tooth, split tooth, and vertical root fracture (VRF) (4).

The initiation site of a physical discontinuity in tooth structure is either the crown or the root. Regardless, longitudinal fractures are generally classified in order of severity, progressing from least to most severe: 1) craze lines, 2) fractured cusp, 3) cracked tooth, 4) split tooth, and 5) vertical root fracture (4,50–53). The term "crack" is used to describe an incomplete propagation of a physical discontinuity that initiates in the crown via craze line or enamel infraction and may progress to fractured cusp, cracked tooth or split tooth with eventual propagation to the root surface in a coronal-apical direction. The 'cracked tooth' is typically found to have subgingival crack extension in a mesio-distal direction, complicating future endodontic and prosthodontic care (26,41).

The term "fracture" can be used to describe an incomplete or complete separation of the material in question and is confined to the root with propagation occurring at any level (54). Tooth fractures are most commonly described as vertical root fractures (VRFs), further defined as a longitudinal fracture of the root, complete or incomplete initiated at any level, usually directed buccal-lingually and are almost entirely the result of prior endodontic treatment (55–58) rather than spontaneous fracture (59). While treatment of vertical root fractures is usually straightforward, it is the initial diagnosis that

is evasive to the clinician due to difficulty in detection, mainly due to their existence within the periodontium and in part because they may bear similarity to other conditions radiographically (8). Improper detection or knowledge of the extent can directly impact short and long-term clinical outcomes.

Technically, a physical separation in tooth structure could encompass both tooth cracks and tooth fracture definitions commonly described throughout endodontic literature. For the purposes of this study, our intention was to evaluate clinically relevant pathologic separation in tooth structure, a crack and/or fracture that would significantly lower overall tooth prognosis – those with radicular propagation that are subgingival and therefore not readily discernable by currently available clinical and diagnostic imaging modalities. The ability to accurately detect such instances would allow diagnosticians and clinicians to make educated decisions on whether preservation or extraction is advised. To allow consistency and clarity, tooth-root cracks and/or fractures evaluated and described specifically in this study will be collectively characterized as "crack/fracture" throughout this present study.

Epidemiology: Prevalence and Frequency

The problem of tooth crack/fracture is by no means a new phenomenon and has been an area of increasing importance in the field of dentistry for several decades (60). The presentation is not uncommon with a full-time general practitioner likely to average at least one case of symptomatic cracked tooth per week (25). In a clinical study evaluating a 6-year period, nearly 10% of patients referred for endodontic consultation or treatment had presence of a cracked tooth (61).

A general increase in prevalence of longitudinal fractures impacting dental care has been observed primarily due to increased tooth retention. With advanced age, teeth are undergoing complex dental procedures and are subjected to repeated occlusal stress. Teeth with restorations have been found to have a 29 times greater risk of cracks than those without (62) and several *in vivo* studies have shown previous endodontic treatment to be a major etiologic factor for tooth fracture (55–58). Outside of iatrogenic procedures,

mechanical behavior of dentin itself has also been shown to change with age. Notable decreases in the maximum flexure strength and energy to fracture indicate that dentin becomes more brittle with age (63). However, older age (>40yrs of age) and presence of past history of operative, endodontic, or prosthodontic treatment are not requirements for increased incidence (64). In addition to decreased rate of dental extraction are the improvements in areas of clinical awareness and diagnosis that include physical procedures enhancing visualization or dental imaging modalities (51). It must be acknowledged that there is a lack of quality epidemiology research studies regarding cracks and fractures in teeth. Recently, the AAE has established a special committee to help facilitate further emphasis and to aid in research design in this under-reported area (5). The subject has continually been identified as a top research priority by the AAE foundation (65).

Detection: Cracks and Fractures

Visual – Direct Observation

Clinically, a patient's signs, symptoms and radiographic appearance of cracks/fractures will often mimic marginal periodontal bone loss or apical periodontitis with radiographic features such as a "halo"-type lesion or narrow, deep periodontal probings that can create difficulties in obtaining definitive diagnoses (36,37). These clinical diagnostic aids can usually suffice in diagnosis of complete longitudinal fractures of the crown or root. However, more challenging diagnostic situations present when there is high suspicion of an incomplete fracture (41) or vertical root fracture (VRF) (1). Periapical sensibility tests may not elicit pain if the pulp is vital, as the crack/fracture may have only early, sub-clinical propagation. If the direction of the percussion test creates separation of the crack and the periodontal ligament is stimulated, then pain may result and diagnosis achieved more readily(35).

Visual inspection for cracks/fractures with a dental operating microscope alone, even with 35x magnification, have been reported to yield lower than expected sensitivity, specificity, and accuracy levels (66). Other enhanced clinical inspection methods revolve

around techniques used to amplify or clarify visual representation such as vital staining via methylene blue and direct light source transillumination (26), with a higher detection achieved when both methods are employed for detection of apical root cracks (67). If a crack is present, the air space will re-direct light and the tooth structure past the crack will appear dark (4). Occasionally, restorations may warrant removal and in some cases an invasive access cavity is needed for full evaluation of the crack extension into the pulp chamber via direct visualization with a dental operating microscope.

Simple clinical diagnostic aids are unreliable when coronal cracks extend below the gingival attachment apparatus, into radicular dentin, and are nearly impossible when apical-coronal fracture extension terminates prior to the gingival attachment as in the presence of VRFs. To date, direct visualization of the root and crack/fracture via invasive surgical flap exposure is the only definitive method for evaluating extent and presence or absence (1,7–9).

Imaging – Indirect Observation

2D Imaging

A review of classic and modern literature concludes that conventional imaging certainly has limitations (7–9). Tamse et al. described the typical radiographic appearance of the resulting bone loss after crack/fracture progression around mesial roots of mandibular molars with vertical root fracture as “halo”- or “periodontal”-type radiolucencies but maintains that definitive diagnosis of the actual crack/fracture can only be made with exploratory surgery (68). Conventional 2D radiographic imaging techniques fail in their ability to accurately visualize VRFs and incomplete cracks due to numerous shortcomings with a 2D projection. Detection of early incomplete cracks or fractures is difficult as superimposition of adjacent and overlying anatomic structures is often encountered. Direct alignment of the x-ray source with the plane of the fracture is required for optimal visualization (69), a problem compounded by the typical mesio-distal initiation pattern observed in coronal-radicular cracks (64).

3D Imaging – Ionizing Radiation-Based

CBCT has been assessed in numerous studies for the detection of longitudinal cracks in teeth (70). It is currently advocated as the image modality of choice when clinical and 2D radiography are inconclusive in detection of VRFs due to its ability to study the suspected tooth and associated supporting bone in the axial plane (15). However, CBCT images do not usually directly visualize the cracks or fractures themselves but rather the end result of bone destruction and periodontal ligament space enlargement surrounding the crack (71,72). The AAE and AAOMR 2015 joint-position paper states that "CBCT should not be used routinely for endodontic diagnosis or for screening purposes in the absence of clinical signs and symptoms." And further, "Clinicians should use CBCT only when the need for imaging cannot be met by lower-dose two-dimensional radiography" (13,15). Given the following factors: 1) radiation used in medical and dental diagnostic X-ray imaging exceeds 15% of the average annual effective dose-equivalent of U.S. individuals from all sources, 2) health-care associated radiation is second only to natural background radiation exposure, 3) the highest manmade source of radiation exposure is dental and medical imaging, and 4) dental X-ray imaging is subject to dental material-related artifacts; clinicians must always allow the patient to make an informed decision while clinically weighing the risk vs. benefit of this more invasive diagnostic aid (73).

Aside from increased radiation dosage, spatial resolution of CBCT is notably less than modern 2D digital receptors, 2 line pairs per millimeter (mm) vs. 7-25 line pairs per mm respectively. Furthermore, while 3D imaging allows visualization without superimposition of anatomical structures, nearly all 3D imaging modalities are liable to a degree of artifact (74). Beam hardening and scatter are the main artifacts present in CT imaging where reconstruction of a projection data set is a requirement prior to data volume review. Clinically, the presence of any radio-dense dental material or extra-oral material (high noble or noble metal alloys, amalgam, implants, silver points, and gutta-percha) can create significant scatter artifact composed of radiopaque lines producing bands of light and dark streaks in image reconstruction. Beam hardening artifacts present

as dark streaks and bands that appear near the periphery of metallic boarders. These artifacts degrade overall image quality and simulate possible pathosis, conceivably leading to false positives (75). Attempts to decrease image artifacts associated with root filling materials have been successful, but frequently require clinically invasive and costly re-treatment procedures aimed at removal of these materials prior to scanning (76).

Adding to the difficulty in interpreting images with notable artifact, the presence of multiple restorations directly correlates with incomplete fracture incidence in the coronal radicular segments – leading to questionable image quality. A clinical study evaluating incomplete tooth fractures associated with diffuse longstanding orofacial pain demonstrated that 89% of the fractured teeth occurred in heavily restored teeth (77). Previous history of root canal treatment also compounds the diagnostic challenge. A clinical survey evaluating over two-thousand fractured teeth in nearly one-hundred patients found that the presence of obturation material is the principle clinical feature associated with root fracture (55). An *in vivo* analysis of root-filled teeth, CBCT imaging used for VRF detection was found to produce significant streaking artifact caused by radiopaque root fillings, which may mimic a crack/fracture leading to a higher false-positive rate (lower specificity) (78).

Ex vivo research has demonstrated that both two-dimensional (digital periapical) and three-dimensional (limited FOV CBCT) X-ray based imaging are comparatively unreliable for detection of simulated incomplete VRFs (17). In examining the *in vivo* diagnostic accuracy of the same two modalities, there was no significant difference between two-dimensional imaging and CBCT in regard to sensitivity and specificity of vertical root fracture detection, both having comparatively poor sensitivity (0.16 and 0.27 respectively) and comparably high specificity (0.91 and 0.83 respectively) (17,79). The AAOMR and AAE 2015 position statement concludes by heeding caution in interpretation of sensitivity, specificity, and accuracy results from studies involving the use of CBCT for detection of vertical root fractures as the size of fracture, presence of artifacts caused by radio-dense filling materials, and spatial resolution of the CBCT system are all dependent variables (13).

3D Imaging – Non-Ionizing Radiation-Based

Near-Infrared Range (NIR)

Translucency of teeth in the near-infrared range (NIR) employs Light Emitting Diode (LED) technology for imaging teeth via a NIR (850nm) source and an intraoral camera permitting a non-ionizing and safe approach to rapid dental evaluations that may have applications for diagnosing deep and superficial cracks (80). However, the technology is limited in that it will only aid in visualization of areas that the light source can be applied, i.e. those crack/fractures that appear supra-gingival which is not the aim of the present study.

Ultrasound

Ultrasound imaging has shown early promise detecting hard tissue discontinuities under existing radio-dense filling materials due to its short wavelength in hard tissue and resulting high resolution. The technology is based on physical acoustics producing an echo that is returned and registered as a linear measurement. The altered acoustics provided by cemental layers and other foreign restorative materials may not be easily accounted for and further limitations have been encountered with angle-dependence of signal transducer preventing decreased validity in more geometrically complex situations found commonly in teeth (81). Furthermore, it is similar to NIR technology in that its applications appear limited to supra-gingival dental tissues.

Optical Coherence Tomography (OCT)

Tiny object detection via OCT has led to the development of dental applications, to include use as a detection agent for micro-fractures, providing a potentially powerful noninvasive method for diagnosing cracks (82). Swept source OCT (SS-OCT) has been shown to obtain subsurface cross-sectional images that are more sensitive than earlier systems, enabling micron-level resolution (83). Imaging via optical coherence tomography is poorly suited for deep crack/fracture detection that specifically involves

the radicular tooth surface due to the limited, shallow penetrating depth of approximately 3mm (84); therefore its use should be restricted to the coronal tooth structure.

Magnetic Resonance Imaging (MRI)

MRI may be an alternative diagnostic imaging method for determining the presence and extent of root cracks and fractures, due to more advantageous contrast, acquisition of a three-dimensional data set, inclusion of useable information about the soft tissues, and avoidance of ionizing radiation (19).

The source of an MR signal in clinical scanners are the protons located in water molecules. Densely calcified enamel and dentin have relatively low amounts of water when compared to other structures within the human body, resulting in small amounts of MRI signal coming from these tissues. Furthermore, the crystalline structure of these densely calcified tissues constrains the movement of water molecules, which decreases the proton relaxation time and shortens the time available to detect the MRI signal. When a tooth has a crack or fracture, a twofold effect occurs; a) more water is present in this discontinuity of tooth structure (i.e. more signal) and b) the water is less restricted within (i.e. longer time to detect signal) (19). Due to this significant increase in signal with cracks or fractures and acceptable contrast to noise, even a narrow gap in tooth structure smaller than the size of an image voxel can cause an observable intensity contrast, a phenomenon referred to as partial volume effect (20). Thus, the voxels in the area of a crack need only gain a small amount of signal to appear bright and therefore be identified visually in the resultant image amongst a very low signal (*a.k.a.* dark) aspect of the densely calcified tissues. This characteristic, which is advantageous with MRI, is one of the limitations experienced with x-ray based imaging techniques. The contrast is low when using ionizing radiation because little relative change occurs in the mineral concentration within a cracked or fractured tooth. This is why voxel sizes comparable with crack thickness are required to detect a tooth discontinuity when using ionizing radiation, which translates to only the detection of larger cracks and fractures imaged with CBCT (19).

In addition to limitations in contrast, image artifacts from commonly encountered dental materials such as gold, amalgam and root filling materials that appear in CBCT may obscure neighboring structures, as well as cracks/fractures in a radial manner (6,85). These image artifacts are notably absent in MRI (86). Hence, MRI may have increased sensitivity to detect tooth-root cracks and fractures.

In the past, conventional MRI visualization of teeth has been limited by the inability to detect the fast decaying signals from teeth that are a direct result of the highly restricted molecular motion of water found in these densely mineralized tissues (86). An MRI technique called Sweep Imaging with Fourier Transform (SWIFT) has overcome many of the inherent difficulties of conventional MRI (21) with detecting fast-relaxing signals from densely mineralized dental tissues (22). SWIFT MRI has the ability to obtain isotropic resolution with minimal acoustic noise; an acoustic level so low that ear protection is usually not needed during scanning (87).

Previous Associated Dental Research

The imaging component utilized in this study was based at the Center for Magnetic Resonance Research (CMRR) at the UMN (UMN), which has a long-standing interest and success in developing MRI technology. This is evidenced by the Center's involvement in pioneering functional magnetic resonance imaging (fMRI) and continued development in the field via the Human Connectome Project (http://www.humanconnectomeproject.org), to highlight a couple examples. Relevant to the present study, researchers at the UMN previously demonstrated the ability to use SWIFT MRI to obtain MR signal from densely mineralized tissues (21), visualize small structures in teeth (accessary canals and cracks), and acquire *in vivo* images of teeth (88). This research has allowed continual improvements to this imaging technology for dental application with the development of an intraoral radiofrequency coil, which allows for higher image resolution, shorter scanning times, and capture of images of tissues that interest the dental professional (89). To prove the feasibility of detecting cracks in teeth, past research at the UMN CMRR involved acquiring SWIFT MRIs of extracted cracked

teeth using the same imaging parameters previously used in patient imaging to mimic "*in vivo* conditions" (intraoral coil with custom oral radiofrequency (RF) coil, field of view=120x120x120mm^3, acquisition=3.5 minutes, band width=100kHz via 90cm, 4-T magnet, 0.27mm isotropic voxel size) (**Figures 10a-c, Figure 12a**). Imaging was conducted on a tooth that was extracted from a patient seeking endodontic care because it was deemed non-restorable due to the presence of cracks within.

The thickness of the cracks was determined by microCT and decreased in width from the coronal to apical direction until transitioning to sound calcified tissue. This naturally provided a situation where the detectability of cracks depended on width. It was found that cracks of ≥20 μm are reliably visible in images with contrast-to-noise ratio (CNR = SNR crack-SNR dentin) around 5. This was encouraging as it demonstrated cracks/fractures can be detected in images even though the physical thickness is about 10 times less than the size of image voxel. In comparison, CBCT in-vitro accuracy has demonstrated a lower crack detection threshold, with a significant decrease in detection of vertical root fractures (VRFs) ≤50 μm compared to those ≥50 μm (17).

OBJECTIVES

Given that i) the location of cracks/fractures can have a significant impact on prognosis of teeth ii) challenges remain in determining the presence of cracks/fractures in teeth with x-ray-based imaging systems, iii) non-ionizing imaging modalities are preferred over ionizing modalities for detecting abnormalities in teeth, iv) MRI techniques have inherent advantages in relation to x-ray based systems, and v) recent advancements in MRI technology have increased image quality at clinically relevant scan times suitable for dental applications (21,22); the following specific aims were proposed:

1) Develop MRI criteria for root crack/fracture identification in human teeth,
2) Measure intra- and inter-rater reliability for crack/fracture detection using SWIFT MRI and limited FOV CBCT, and

3) Assess the sensitivity and specificity of MRI and CBCT for the detection of tooth-root cracks/fractures when compared to known crack/fracture status.

HYPOTHESIS

Both SWIFT MRI and limited FOV CBCT will have substantial (κ>0.6) intra-and inter-rater reliability. MRI will have greater sensitivity for crack/fracture detection than CBCT, while CBCT will have greater specificity than MRI.

MATERIALS AND METHODS

Prior to commencement, the study protocol was approved by the Institutional Review Board (IRB HSC: 1601E83241; Principle Investigator: Donald Nixdorf) of UMN, Minneapolis, MN.

A collaborative team of researchers assisted in the completion of the study and will be referenced herein via abbreviated text: (Dr. Tyler Schuurmans [TS], Resident, Graduate Endodontics, Division of Endodontics, UMN School of Dentistry; Dr. Donald Nixdorf [DN], Associate Professor, Department of Diagnostic and Biological Sciences, Diplomate–American Board of Orofacial Pain, UMN School of Dentistry; Dr. Alan Law [AL], Adjunct Associate Professor, Department of Restorative Sciences, UMN School of Dentistry; Dr. Brian Barsness [BB], Endodontist; Clinical Assistant Professor, Department of Restorative Sciences, UMN School of Dentistry; Dr. Samantha Roach [SR], Clinical Assistant Professor, Department of Restorative Sciences, Diplomate–American Board of Endodontics, UMN School of Dentistry; Dr. Laurence Gaalaas [LG], Oral and Maxillofacial Radiologist, Clinical Assistant Professor, Diplomate–American Board of Oral & Maxillofacial Radiology, School of Dentistry, UMN School of Dentistry; Dr. Djaudat Idiyatullin [DI], Assistant Professor, Center for Magnetic Resonance Research, Department of Radiology, UMN; Lei Zhang [LZ], Research Fellow, Bio statistical Design and Analysis Center (BDAC) at the UMN's Clinical and Translational Science Institute (CTSI).

De-identified extracted human adult teeth used throughout the training and calibration exercises and as control specimens in the experimental study were obtained from previous waste tissue generated by the UMN Oral and Maxillofacial Surgery clinic. De-identified extracted teeth used for the convenience sample in the experimental study were previously collected as de-identified waste tissue generated by an endodontist in private practice [AL]. All experimental teeth were extracted as atraumatically as possible and immediately stored in 10% neutral buffered formalin to preserve the physical characteristics of the teeth and to maintain moisture content.

Experimental Method

The research pertaining to this study followed Frybach & Thornbury's hierarchical model of assessing new diagnostic imaging methods, a diagnostic approach that has the intent of providing the clearest images, allowing the most accurate diagnoses in a globally effective and efficient manner (73).

The lowest level (Level 1) is the technical aspect of transmission of information – a description of the physical imaging process. Simply put, what can one resolve within dental MR imaging and what is observed when evaluating the image. Level 2, "diagnostic accuracy efficacy" includes both the image and the interpretation by the person which in this study was structured as a reiterative process that involved collaborative group training sessions. Level 3, "diagnostic thinking efficacy" can be summarized as the extent to which the image was thought to be helpful in aiding a clinical diagnosis – specifically presence or absence of a crack/fracture. Level 4, "therapeutic efficacy" describes the image helpfulness in planning the management of a case and potential ability for it to change the clinicians' prospective treatment choice (73) – i.e. possible consideration of dental extraction.

This study assessed the "diagnostic accuracy efficacy" of detecting the presence of a crack/fracture in a tooth root. The primary hierarchical aim was to address level 2 in assessing this new imaging modality, dental SWIFT MRI, via an *ex vivo* model. In

addition, limited consideration was given to level 4 in shaping panel members' critical thinking as it applies to hypothetical clinical decision making.

Training and Calibration

Sample Selection and Preparation

Screening for selection of a suitable *ex vivo* sample to serve as a calibration specimen was directed at identifying a human tooth that contained a multitude of common dental restorative and prosthetic materials. Such a sample would represent a challenging real-world situation likely to confront diagnosticians due to substantial image artifact associated with radio-dense filling materials. In addition, a tooth containing these elements would also allow for calibration of rater image interpretation and provide for any needed adjustments of scanning and image parameters to improve future diagnostic quality – regardless of the presence of dental restorative or root filling materials.

A previously extracted, de-identified and fully intact maxillary right first premolar with three roots was confirmed to have radicular cracks/fractures following magnified visual inspection with a dental operating microscope (Global Surgical™ Corporation, St. Louis, MO, USA) at 10Xs magnification, transillumination and vital staining (methylene blue, 1% - Vista Dental Products, Racine, WI, USA) (**Figures 2a,b**) (**Figure 3a,b**).

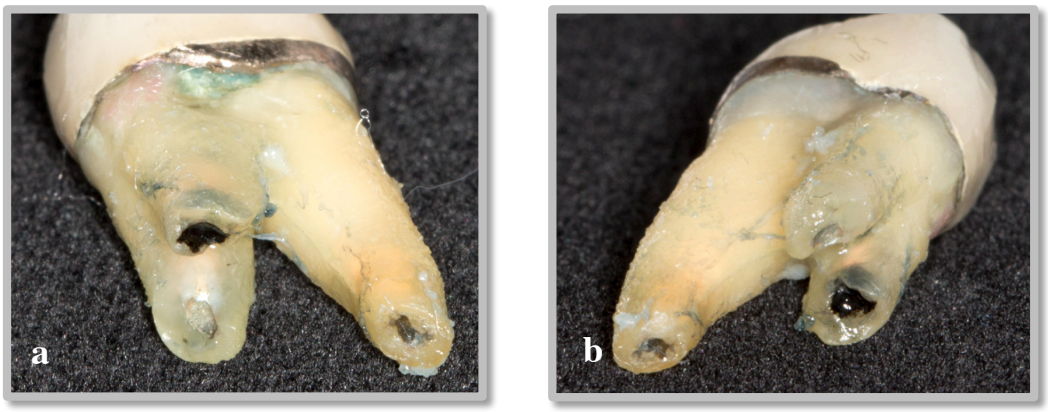

Figures 2a,b. Calibration Specimen: previously extracted, intact Tooth #5 with presence of three roots and a coronal full-coverage porcelain fused to metal (PFM) restoration. Inspection revealed evidence of previous NSRCT and SRCT (RER/REF).

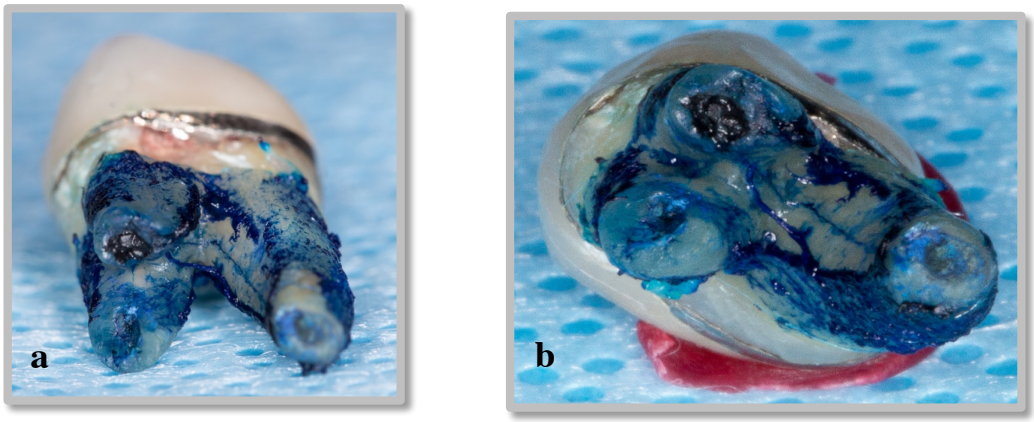

Figures 3a,b. Calibration Specimen: previously extracted, intact Tooth #5 with presence of three roots and a coronal full-coverage porcelain fused to metal (PFM) restoration. Inspection revealed evidence of previous NSRCT and SRCT (RER/REF). Vital staining (methylene blue, 1% - Vista Dental Products™) was utilized to enhance visual detection of multiple vertical root fractures.

Filling material contents and evidence of previous non-surgical root canal treatment (NSRCT) and surgical root canal treatment with root end resection and root end filling (SRCT with RER/REF) were confirmed by 2D digital radiographic survey analysis (**Figure 4**) via an RVG 6100 Kodak sensor and software (Carestream, Rochester, NY). Inspection yielded multiple aspects that were considered ideal characteristics: 1) presence of multiple dental restorative and prosthetic materials (amalgam alloy core, porcelain fused to metal crown), 2) presence of multiple intracanal endodontic filling materials (gutta-percha, ZOE-based endodontic sealer, and a modern bio-ceramic material, grey mineral trioxide aggregate (GMTA ProRoot™), 3) presence of prior surgical endodontic treatment via apical root-end resection, root end-preparation, and root-end filling via a modern bio ceramic filling material (e.g. ProRoot™ GMTA), 4) multiple vertical root fractures confirmed via visual inspection, and 5) a morphologic tooth type (maxillary premolar) commonly encountered when diagnosing vertical root fractures in previously root-canal treated teeth (90).

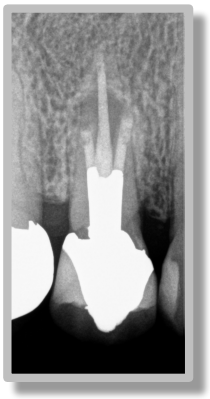

Figure 4. Periapical radiograph of calibration specimen (RVG 6100 Kodak sensor and software (Carestream, Rochester, NY)).

Tooth moisture was maintained during manual inspection by supporting the tooth with a 2x2cm cotton gauze saturated with tap water. After inspection, the tooth was then placed in a 14.8 ml (diameter: 21mm; length: 70mm) stock glass laboratory vial (Acme Vial & Glass Co., Inc., Paso Robles, CA, USA) in a crown-down orientation and filled

with tap water. 2x2cm cotton surgical gauze were then packed around the roots to secure the coronal-apical tooth orientation, minimize any future bodily movement and to maintain physiologic moisture throughout sample transport, mounting and imaging. The plastic vial cap was punctured to eliminate the presence of any residual trapped air column during cap affixation to best mimic the continually moistened physiologic oral environment.

Imaging

X-ray-based

3D MicroCT (μCT) was utilized to establish crack/fracture ground truth in the calibration sample (44,91). MicroCT (Metrix , model XT H 225; Nikon Metrology, Brighton, MI) images were obtained at the UMN School of Dentistry, within the Minnesota Dental Research Center for Biomaterials and Biomechanics (MDRCBB) in one scan using 90 kV, 90μA, 708ms of exposure, 720 projections and four frames per projection. The resolution of the specimens after reconstruction was 7μm (**Figure 5**). To adhere to the required scanning protocol, the tooth was briefly removed from the tap water-filled vial to facilitate proper MicroCT scanning and afterward, immediately returned for storage.

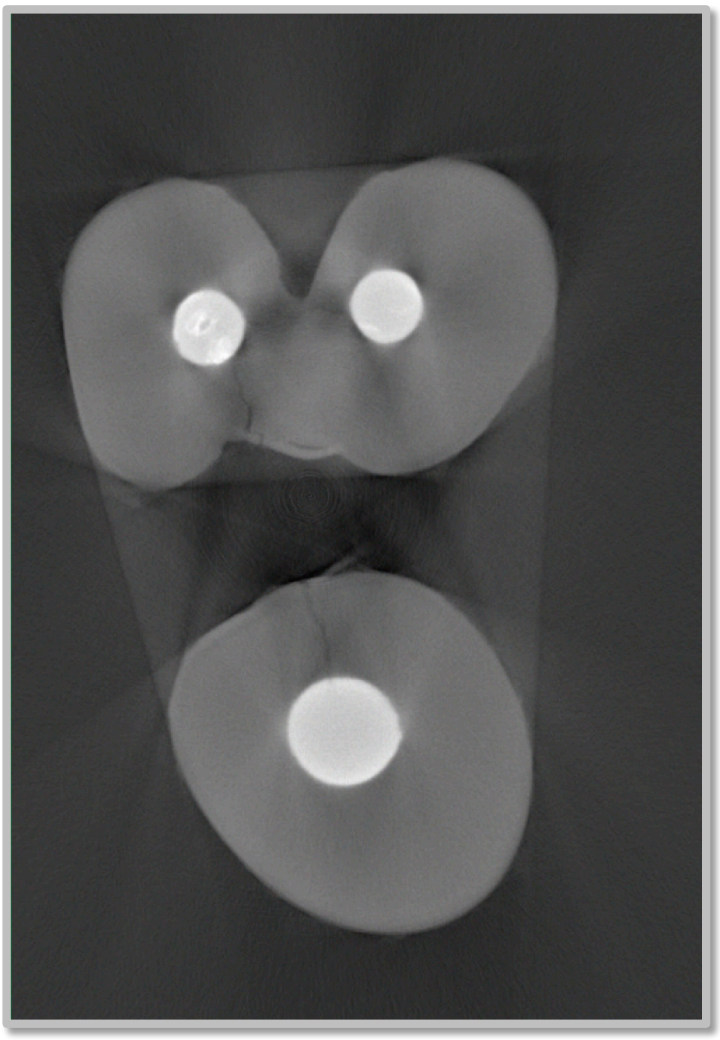

Figure 5. Calibration specimen: selected axial image slice taken from the 3D MicroCT image volume with notable cracks/fractures. Image from a previously extracted, intact Tooth #5 with presence of three roots and a coronal full-coverage porcelain fused to metal (PFM) restoration. Inspection revealed evidence of previous NSRCT and SRCT (RER/REF).

3D limited FOV CBCT was used as a clinical reference standard in the study. CBCT images were acquired in the graduate endodontics department at the UMN School of Dentistry via a commercially available unit (Carestream – CS 9000, Rochester, NY). A custom-fabricated scanning platform was constructed via mounting a 2x4" wood board to the existing proprietary (CS 9300) plastic platform to facilitate consistent vial positioning, orientation and to reduce vial movement during scanning (**Figure 6**).

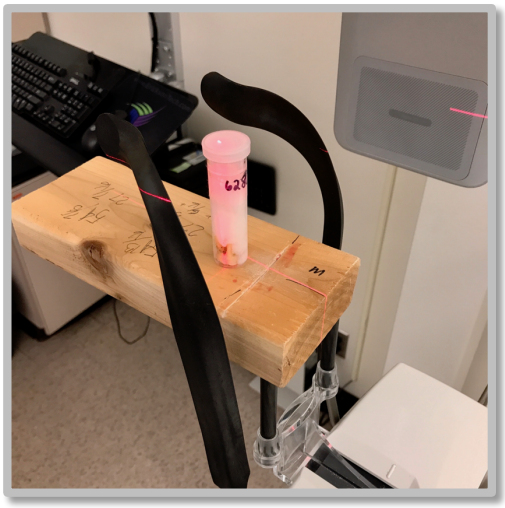

Figure 6. Custom-fabricated wood scanning platform attached to the CS 9000 Limited FOV CBCT scanning unit.

CBCT scanning parameters were determined by an experienced, board-certified OMF radiologist [LG] and were completed by imaging 1 tooth/scan, with a field of view 5x3.75cm at 5mAs^{-1} for 10.8s and 68 kV with a nominal isotropic voxel size of 0.076 mm. The CBCT images were optimized via the CS 9000 3D imaging v3.2.13 software platform (Carestream – CS 9000, Rochester, NY) (**Figure 7**).

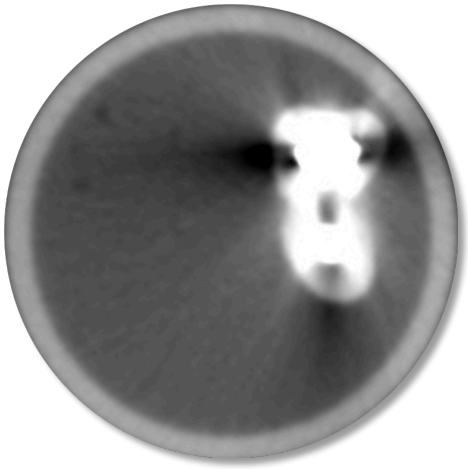

Figure 7. Calibration specimen: selected axial image slice taken from the Limited FOV CBCT image volume with notable presence of metal streak artifact. Image from a previously extracted, intact Tooth #5 with presence of three roots and a coronal full-coverage porcelain fused to metal (PFM) restoration. Inspection revealed evidence of previous NSRCT and SRCT (RER/REF).

MR-based

In the present study, MR imaging served as the experimental or test standard. MRIs were obtained at the Center for Magnetic Resonance Research (CMRR) at the UMN. All MRI experiments were performed in a 4.0-Tesla (T) 90cm bore whole-body human magnet system (Oxford, UK) equipped with an Agilent DirectDrive console (Palo Alto, CA) as outlined in previous associated research (86). The system computers were connected by a 10 G/s Ethernet network link allowing rapid transfer of image data to the data center for post-processing, analysis, and storage. The scanner was equipped with Siemens SC72 gradient coils with a maximum gradient 50mT/m and rise time 500 microseconds. A custom-fabricated, single-loop, 50mm-diameter intraoral coil was used for radiofrequency transmission and signal reception. The RF coil had undergone prior testing in *ex vivo* and *in vivo* experiments (12) and was utilized for imaging the teeth in this study providing a field of view=120x120x120mm^3 (**Figure 10a-c**)

In the SWIFT MRI sequence, (21) radiofrequency excitation was performed with an amplitude- and frequency-modulated pulse, commonly called the "hyperbolic secant pulse", with a stretching factor of 2, a time–bandwidth product of 64, an excitation bandwidth of 100 kHz and flip angle (θ) of 8°. Data were collected in 64 gaps (of 7.4μs each) in the RF pulse and after the pulse, 192 samples were acquired without gaps. The repetition time, including the 0.64-ms pulse length, was 2.6ms. Data in k-space consisted of 64,000 spokes with termini describing the isotropically distributed points on a sphere. After acquiring a full set of frequency-encoded projections, 3D images were reconstructed with CMRRpack v. 0.45b SWIFT software (92). The gradient-echo (GRE) MRI acquisition used Cartesian k-space sampling with 256 readout points with 10 microsecond (ms) dwell time and 192X192 phase encodings. Repetition time and TE values were 5.46 ms and 2.75 ms, respectively, and θ was 15°. The field of view for all MRI experiments was 12x12x12cm^3 and the total acquisition time for each experiment was equal to 3.5 min. All MR images were reconstructed to nominal resolution with a 0.27-mm isotropic voxel size. Throughout the training and calibration exercises, assumptions were made by the MRI physicist [DI] and board-certified OMF radiologist [LG] in development of the ideal visual MR imaging parameters (**Figure 8**).

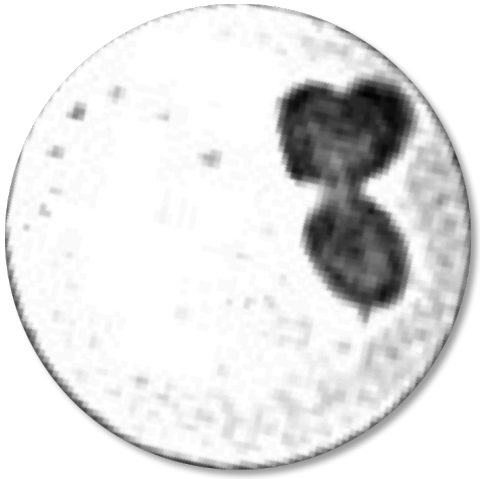

Figure 8. Calibration specimen: selected axial image slice taken from the SWIFT MRI image volume with notable absence of metal streak artifact. Image from a previously extracted, intact Tooth #5 with presence of three roots and a coronal full-coverage porcelain fused to metal (PFM) restoration. Inspection revealed evidence of previous NSRCT and SRCT (RER/REF).

Development of MRI-based Criteria

Experimental MR images were evaluated by six dentists (experienced board-certified or board-eligible endodontists n=3 [AL] [BB] [SR]; a board-certified OMF radiologist n=1 [LG]; a board-certified TMD/Orofacial Pain specialist n=1 [DN]; a graduate endodontic resident n=1 [TS]) and an MRI physicist [DI] in collaborative training sessions. MR images were simultaneously cross-compared to the corresponding MicroCT and limited FOV CBCT images to aid in the groups' development of an MRI-based criteria with regards to how cracks and/or fractures in teeth appear with this new dental imaging modality – ***Specific Aim 1*** of the study. This was a reiterative process inclusive of three separate calibration sessions to aid in the development of this new MR-based imaging criteria.

Throughout the training exercises and the experimental study, raters were allowed to manipulate basic imaging settings e.g. scrolling through axial slice position, image brightness, contrast, zoom and panning adjustments – consistent with basic digital

radiography viewing software. Each 3D image review was standardized by restricting slice view and orientation entirely to the axial plane as increased sensitivity of CBCT in crack/fracture detection in CBCT appears to be largely due to the ability to evaluate in the axial plane (17,93). Following review and interpretation of the entire radicular axial image slices within each image set, raters were instructed to declare the presence or absence of a crack/fracture on a sheet of paper (dichotomous variable: crack/fracture present – "yes" or "no") as the primary outcome (***Specific Aim 2 and 3***) of the study. Secondly, when a sample was designated as having a crack/fracture, the best representative axial slice range was recorded and a drawing corresponding to the observed axial root slice crack/fracture position was completed as an exploratory outcome.

To fulfill the primary objective of evaluating tooth-root cracks and fractures, prior to rater presentation, DICOM image stacks were cropped by a blinded operator [DN] to produce radicular images devoid of enamel or prosthetic crown margins. Digital image editing for all modalities to include cropping and image registration for image standardization and DICOM stack exporting were completed via the open-source ImageJ™ v1.51f software package (National Institutes of Health, USA). Rater image viewing, image manipulation and interpretation were completed via Windows-based RadiAnt™ DICOM v3.4.2.13370 viewer (64-bit) software package (Medixant, USA).

Calibration Exercise

In accordance with earlier described procedures, intact, de-identified previously extracted teeth underwent screening and evaluation to confirm presence of tooth-root crack(s)/fracture(s). Fourteen teeth were included to maximize rater exposure to the MR appearance of cracks/fractures for efficient image interpretation and training exercises. Five representative sample teeth were chosen by group consensus and MicroCT scans were obtained. MR image slices were simultaneously cross-compared to corresponding MicroCT and limited FOV CBCT axial slices and to digital high-resolution photographs of the external tooth surface to establish ground truth. These concurrent image

comparisons served to stimulate further group discussion with regards to the appearance of tooth-root cracks/fractures within this new dental imaging modality. For questionable cases where disagreement of diagnosis existed, discussion ensued to achieve a consensus of the criteria. Throughout this collaborative training process, the MRI-based criteria were altered in a reiterative process while also changing the MRI imaging pipeline in accordance with the expert opinion of an MRI physicist [DI] and an oral and maxillofacial radiologist [LG].

MRI-based criteria were defined as 1-2 sharply-delineated, high-signal (bright/white) line shape(s) that must be visible on multiple contiguous axial image slices. The line shape(s) must present as: single entities or parallel pairs in close proximity, or pairs in close proximity exhibiting convergence or divergence extending from the external boundary of the tooth to the pulpal cavity (*see* ***Appendix I***). The calibration sample MR, CBCT, and MicroCT images were utilized in development of familiarity with both the task and process prior to commencing with the experimental study.

Experimental Study

The development of this section was performed in conjunction with staff [LZ] from the Bio Statistical Design and Analysis Center (BDAC) at the UMN's Clinical and Translational Science Institute (CTSI).

Sample Size Determination

The Kappa statistic was used to determine the level of agreement to assess reliability. A kappa of 0.50, which is considered to be moderate agreement (94), is the target level of agreement with the lower limit of the 95% confidence interval (CI) to be 0.50 or greater. With half the extracted teeth with cracks and half without, a total of 32 teeth would be needed in order to achieve 80% power with a 2-sided test, and 43 subjects would be needed in order to achieve 90% power with a 2-sided test (95). We set the acceptable lower limit of 95% CI for sensitivity at 60% and the acceptable lower limit of

95% CI for specificity at 80%. These values were chosen based on other limits set for diagnostic research that were designed to avoid unnecessary false positive rates (96). The tables below display a range point estimates, using a one-sided test, that take into account our target lower limit with a power of 0.80 (97).

Table 1a: Sample size for cases based on sensitivity

Acceptable Lower Limit	**Expected Sensitivity**	**Sample Size Power=0.80**
0.60	0.70	157
	0.75	71
	0.80	**39**
	0.85	24
	0.90	17
	0.95	10

Table 1b: Sample size for controls based on specificity

Acceptable Lower Limit	**Expected Specificity**	**Sample Size Power=0.80**
0.80	0.85	392
	0.90	95
	0.95	**37**

If we expect the sensitivity is 0.80 and the specificity is 0.95, 40 teeth in each group would be ideal to have at least 80% probability for the estimated lower limit of the 95% CI of sensitivity and specificity above; thus being the determining factor for the sample size for the *ex vivo* research.

Sample Selection and Preparation

Over the course of normal practice, patients with teeth that are deemed to be non-restorable following pre- and/or intra-operative diagnosis of a compromising radicular crack/fracture will have these teeth extracted. The diagnosis of crack and/or fracture and subsequent unfavorable prognosis classification are a result of a combination of subjective patient complaints and objective tests that involve varying degrees of invasiveness: periodontal examination, diagnostic imaging interpretation, removal of existing restorations, initiation of endodontic access, and/or surgical flap reflection (4,7–9). Collecting experimental study material in this way best represents the clinical situation: the most common types of teeth presenting with cracks/fractures, occurring in

the most common locations, and in the absence of coronal restorative materials that make it more difficult to visualize cracks/fractures.

Following the results of the training and calibration exercises, teeth previously diagnosed by a board-certified endodontist in private practice with 22 years of clinical experience [AL] as being non-restorable due to compromising cracks/fractures were retained as de-identified study material. Determination of crack status was made clinically, following the diagnostic process outlined in the American Association of Endodontists (AAE) (4). An experimental convenience sample of 29 human adult teeth confirmed post-extraction by visual inspection techniques (previously described in the training and calibration exercises) to have root crack(s)/fracture(s) was then frequency-matched to a control sample of 29 de-identified extracted human teeth later confirmed to be free of radicular cracks and fractures. MicroCT imaging was utilized as an accepted gold or reference standard to assess the presence and extent of cracks/fractures in the calibration sample and in development of the MRI-based imaging criteria (44) but was unavailable for the experimental phase due to cost limitations. Following visual inspection, ground truth for the experimental sample was recorded in an Excel spreadsheet by listing tooth surface and vial specimen number.

Control teeth were frequency matched to the experimental sample based on the following group-wise characteristics: morphology, history of previous NSRCT or SRCT (RER/REF), presence and type of definitive core restoration and/or access temporization, presence and type of extra coronal restoration. If previously root canal treated control teeth could not be located, *ex vivo* NSRCT and SRCT (RER/REF) were completed by a second-year graduate endodontic resident [TS] with six years of prior general dentistry experience via a benchtop preparation sequence. Teeth were held in the operator's hand with a 2x2 cotton gauze moistened with tap water during the entirety of restorative and endodontic treatment to preserve native periodontal ligament (PDL), cementum and root dentine moisture.

Sample glass vials were coded with a randomized 4-digit number and prepared as outlined in the training and calibration exercises to preserve coronal-apical orientation, limit movement during scanning and to limit air-bubble inclusion that was found to

produce MR and CBCT image artifact in the training and calibration sessions (**Figure 9a-c**). Blinded operators ([DI]=MRI; [TS]=CBCT) completed scanning via two 3D imaging modalities: SWIFT MRI (10 Teeth/Scan) as the experimental – via a custom oral radiofrequency (RF) coil, field of view=120x120x120mm^3, acquisition time=3mintues, band width=100kHZ via a 90cm, 4-T magnet, 0.27mm isotropic voxel size (**Figure 10a-c**); and CBCT (1 tooth/scan) as the clinical reference – CBCT scanning parameters were determined by a board-certified OMF radiologist [LG] and were completed by imaging 1 tooth/scan, with field of view=5cmx3.75cm, at 5mAs^{-}1 for 10.8s and 68 kV with a nominal isotropic voxel size of 0.076 mm via CS 9000.

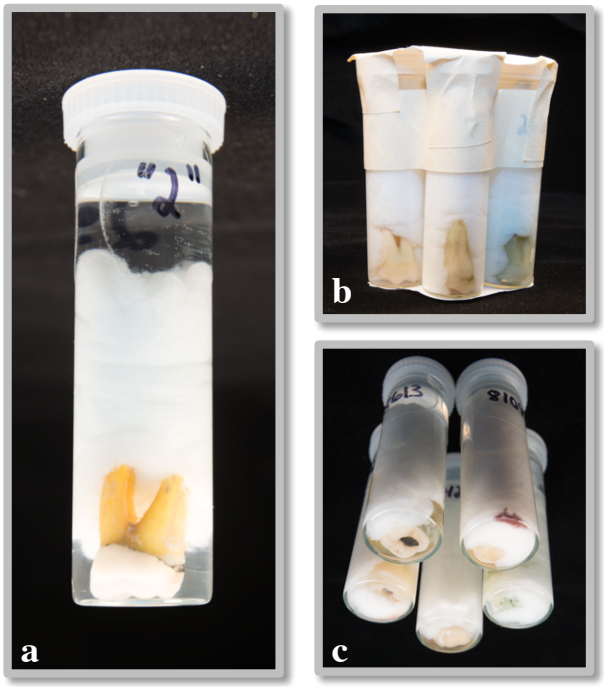

Figures 9a-c. Teeth secured in water-filled glass vials via 2x2cm surgical gauze. To allow equal spacing on the RF coil to facilitate MR imaging, 5 vials were grouped in a circle and secured with tape prior to mounting to the superior and inferior surface of the RF coil.

Each MRI scan included 10 vials in total: 5 superior and 5 inferior to the RF coil. The vials were then wrapped in a plastic bag and secured via masking tape (**Figure 10a-c**). CBCT scanning included 1 vial per scan resting on the previously described custom-fabricated scanning platform to facilitate standardized vial positioning, orientation and to control for vial movement during scanning **(Figure 10a-c)**.

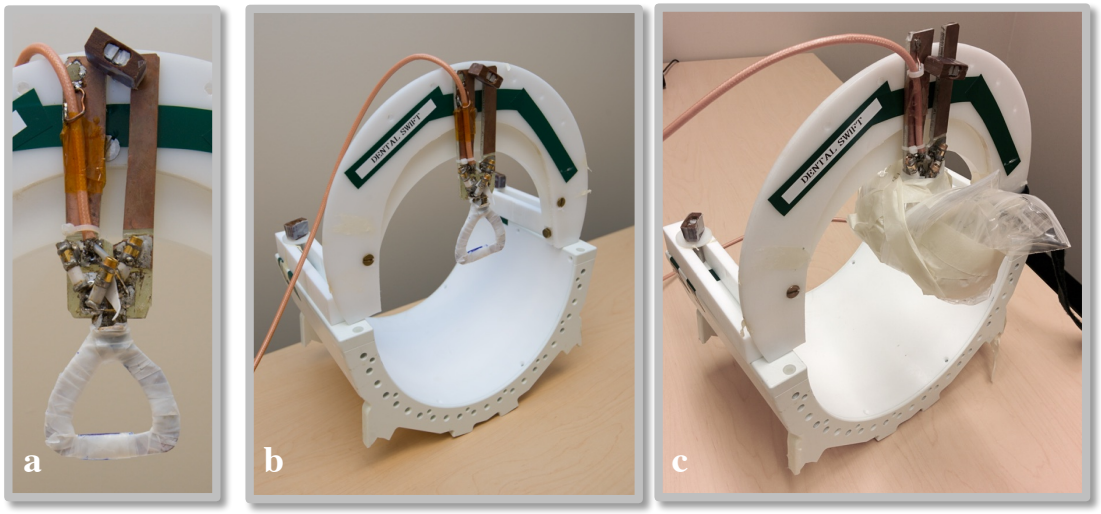

Figures 10a-c. Custom-built, intraoral radiofrequency (RF) providing a field of view=120x120x120mm^3. Each grouping of glass vials (5 vials per grouping, **Figure 9a,b**) was secured to the superior (5 vials) and inferior (5 vials) surfaces of the RF coil via tape to orient the teeth in an orthogonal position, simulating supine patient positioning.

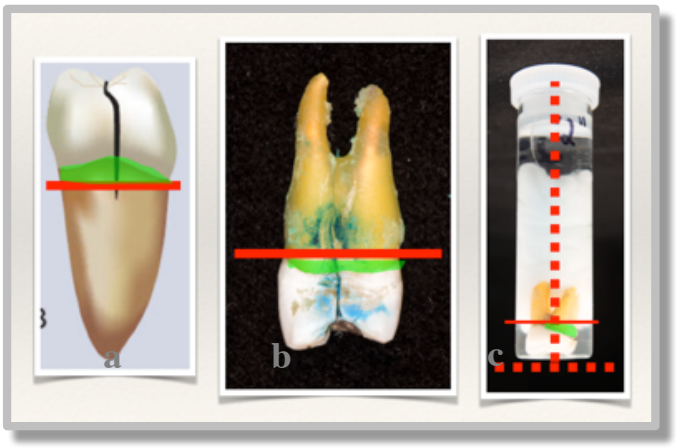

Figures 11a-c. Graphics depicting the anatomic linear cropping method used to produce resulting axial DICOM image sets devoid of enamel or prosthetic crown margins **(a,b)**. Photo depicting variation in CEJ tooth position in vial (**c**). Green highlighted zones indicating potential radicular tooth surface excluded from rater review (**a-c**).

To fulfill the primary objective of the study, prior to rater presentation, DICOM image stacks were cropped by a blinded operator [DN] to produce tooth-root axial plane image stack sections devoid of enamel or prosthetic crown margins (**Figure 11**). Image adjustments and optimization were completed as outlined in the training and calibration exercises. In contrast to CBCT images, MR DICOM image stacks were found to have varying degrees of focus during training and calibration exercises. This inherent, variable image focus within the MR axial image stack could not be continually auto- or rater-adjusted throughout image review due to current software limitations (**Figure 13**). Therefore, a blinded operator [DN] made a subjective determination of the best overall radicular image focus plane for each respective tooth image set prior to presenting to the raters.

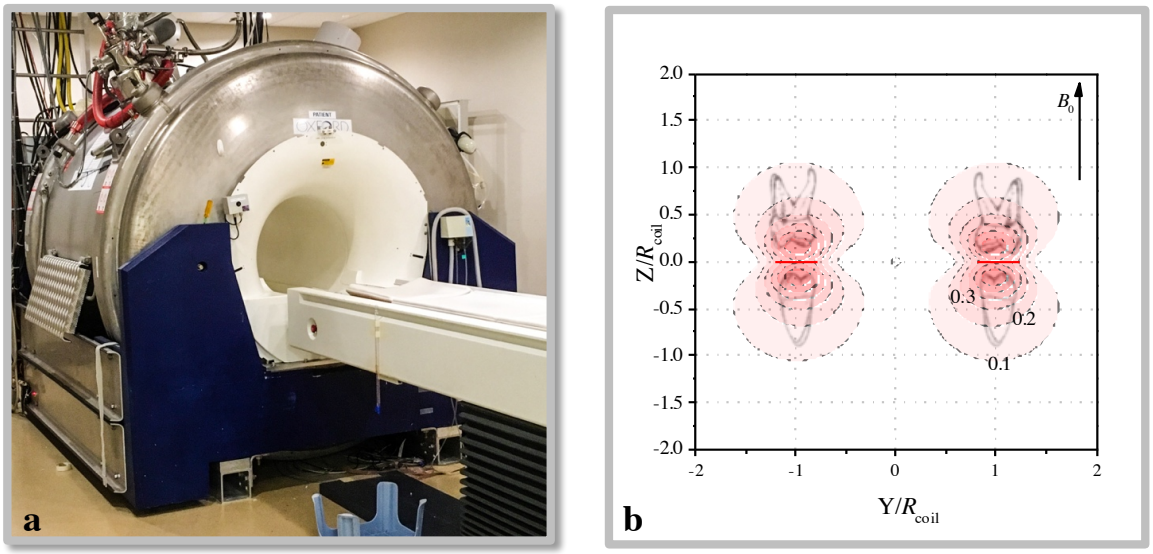

Figures 12a,b. 4.0-Tesla (T) 90cm bore whole-body human magnet system (Oxford, UK) equipped with an Agilent DirectDrive console (Palo Alto, CA). Graphic depicting coil in the occlusal (orthogonal) to the tooth long axis.

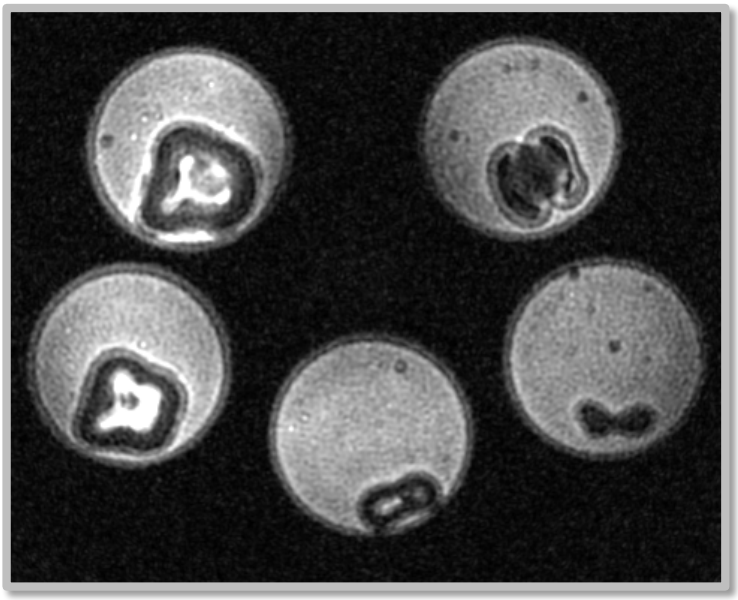

Figure 13. Selected axial slice of a raw SWIFT MRI prior to cropping the image to include only 1 tooth per image set. Note the variable focus within this image, producing an out-of-focus, double-line phenomenon. This phenomenon was taken into account when developing the MRI-based criteria for radicular crack/fracture presentation.

The 29 cracked/fractured experimental samples and the 29 non-cracked/fractured frequency matched controls each had corresponding CBCT and MR images, totaling 116 tooth image sets. The images were randomly batched into one list and the order of image presentation was further randomized with Excel™ software (Microsoft™, Redmond, WA, USA). Images were reviewed as one-tooth per image set with 20% randomly re-tested throughout the same review period to establish intra-rater reliability. Inclusive of re-tested image sets, 140 total image sets were included in the study.

Data Analysis

Four blinded examiners (experienced board-certified or board-eligible endodontists n=3 [AL] [BB] [SR]; board-certified OMF radiologist n=1 [LG]) evaluated the images in one image review session in the undergraduate radiology interpretation area at the UMN School of Dentistry. Dim-light conditions with absence of ambient light and

external noise were standardized across work-stations that included a contrast-calibrated 19" LCD Dell P1913S flat panel monitors with a screen pixel resolution of 1440 x 900 (Dell Inc., Round Rock, TX, USA). One monitor was strictly dedicated to image review while the second was used for digital file management. The review session was unconstrained by time, and raters were allowed as-needed, open-ended breaks to limit fatigue and eye strain. As in the training and calibration exercises, raters were allowed to manipulate basic imaging settings e.g. scrolling through axial slice position, image brightness, contrast, zoom and panning adjustments – via Windows-based RadiAnt™ DICOM v3.4.2.13370 viewer (64-bit) software package (Medixant, USA).

MRI-based criteria for tooth-root crack/fracture previously developed during the training and calibration exercises, and existing criteria for crack(s)/fracture(s) appearance in CBCT (85,98) (*see* ***Appendix I***) were utilized as references available to raters during image review and interpretation. Following review of the entire radicular axial image slices within each image set, raters were instructed to declare the presence or absence of a crack/fracture on a sheet of paper (dichotomous variable: crack/fracture present – "yes" or "no") to fulfill ***Specific Aims 2 and 3*** of the study. Secondly, when a sample was designated as having a crack/fracture, the best representative axial slice range was recorded and a drawing corresponding to the observed axial root slice crack/fracture position was completed as an exploratory outcome that could be utilized in future research (*see* ***Appendix IV***). After 10 image reviews, the rater was automatically prompted to verify that the preceding image numbers matched the data collection sheet number. Raters were then presented with specific post-test questions and a free-response section to gauge study set-up and design. As an exploratory outcome, following the official rating period, each rater was asked what 10 image-sets best demonstrated the ability for SWIFT MRI to detect radicular cracks and fractures. Paper was utilized during rater review for data recording to minimize the distraction of an additional computer monitor.

Following the study, the entire data set was transferred from hard-copy rater sheets into an Excel document (Microsoft™, Redmond, WA, USA) by two independent persons via a double entry method to minimize the presence of in and out errors.

Statistical Analyses

Statistical analyses were conducted using the Statistical Analysis System (SAS) system (v. 9.3; SAS institute, Cary, NC, USA) to compare the two independent imaging modalities, SWIFT MRI and limited FOV CBCT. The 4 examiners' results (dichotomous categorical variable: crack/fracture present – "yes" or "no") for each image set, inclusive of the two independent imaging modalities (CBCT and MRI) were compared to the gold standard (physical detection) using a two-sided chi-square test to determine the sensitivity and specificity of each modality in detecting crack(s)/fracture(s). As previously reported, the ground truth for the experimental cracked/fractured teeth sample included in the study was initially established through clinical diagnosis by a board-certified private practice endodontist [AL] using AAE-based crack/fracture criteria (4). The ground truth for crack/fracture status was determined in the control sample (crack/fracture absence), and confirmed in the experimental sample (crack/fracture) by a second-year graduate endodontic resident [TS] via direct physical inspection as outlined earlier in the study. For each of the sensitivity and specificity measures, 95% confidence intervals (CIs) were computed. Statistical significance was set at œ≥0.05. Diagnostic accuracy and reliability of each examiner and each imaging system for detecting tooth-root cracks/fractures was determined using intra- and inter-rater agreement kappa values. Overall observer agreement was measured using Cohen's kappa and levels of agreement judged using the criteria of Landis and Koch (94).

RESULTS

Training and Calibration Exercises

Quantitative and Qualitative Results

No formal data analysis was performed during training and calibration exercises. The primary outcome of these sessions (***Specific Aim 1*** of the study) was the development of an MRI-based tooth-root crack/fracture criteria via consensus building in a reiterative process.

MRI-based Tooth-Root Crack/Fracture Criteria

The main source of an MR signal is the protons located in water molecules (99). Densely calcified enamel and dentin have low amounts of water and the crystalline structure constrains the movement of water molecules. However, when a physical discontinuity of tooth structure occurs (referenced here as a crack/fracture), more water is present and the water is less restricted, resulting in more MR signal (19). The resultant sharply defined, high-signal line shape creates intense visual contrast, appearing as bright line shapes with three notable presentation types further explained in the criteria outlined below. This variation in visual MRI crack characteristics is dependent upon the degree of MRI focus within a sample image, an inherent variable observed in the development of this imaging modality. For instance, a crack/fracture present in an MRI image may appear both in-and-out-of-focus throughout the extent of that crack. This change in image focus within a reconstructed MR image of dental tissue is the product of local field susceptibility artifact or a change in field distribution commonly encountered when a variation of soft and hard tissues, including dental restorative materials are juxtaposed (19,86).

The first set of MR-based criteria serves to both identify and specify the appearance of high-value line shapes in MRI and define the location of what constitutes a crack/fracture, which for the purposes of this study encompasses cracks and/or fractures that are present on root structure.

Crack/Fracture Criteria:

- *1-2 sharply-delineated, high-signal (bright/white) line shape(s) that must be visible on multiple contiguous axial image slices.*
- *The line shape(s) must present as: single entities or parallel pairs in close proximity, or pairs in close proximity exhibiting convergence or divergence extending from the external boundary of the tooth to the pulpal cavity*

Furthermore, it is important to differentiate cracks/fractures from other commonly encountered pathologic changes in tooth morphology that may be observed in MRI, and

to rule out artifact and possible false positive identification. The following entities should be differentiated from cracks/fractures:

- *Aberrations in dental anatomy or morphology which may include*
    - *Accessory, lateral or secondary pulp canal(s)*
    - *Canal ramifications*
- *Physiologic or pathologic processes which may include*
    - *Root Resorption (Inflammatory, Replacement, Surface, Cervical, External, Internal)*
    - *Caries*

Experimental Study

Quantitative Results

The results indicate that both MRI and limited FOV CBCT imaging have comparably high specificity (0.83 and 0.90, respectively) and poor sensitivity (0.59 and 0.59, respectively) (**Table 2**), with both modalities demonstrating similar, overlapping 95% confidence intervals (CI) (**Figures 14,15**).

Variable	Variable	Statistics	Sensitivity	Specificity
CBCT	A	Est (95% CI)	0.59 (0.39, 0.76)	0.93 (0.77, 0.99)
		P-value	0.46	<0.01
	B	Est (95% CI)	0.55 (0.36, 0.74)	0.76 (0.56, 0.90)
		P-value	0.71	<0.01
	C	Est (95% CI)	0.59 (0.39, 0.76)	0.79 (0.60, 0.92)
		P-value	0.46	<0.01
	D	Est (95% CI)	0.66 (0.46, 0.82)	0.66 (0.46, 0.82)
		P-value	0.14	0.14
	Consensus	**Est (95% CI)**	**0.59 (0.39, 0.76)**	**0.90 (0.73, 0.98)**
		P-value	**0.46**	**<0.01**
	Consensus (excl. rater A)	Est (95% CI)	0.59 (0.39, 0.76)	0.79 (0.60, 0.92)
		P-value	0.46	<0.01
	Consensus (excl. rater B)	Est (95% CI)	0.62 (0.42, 0.79)	0.90 (0.73, 0.98)
		P-value	0.26	<0.01
	Consensus (excl. rater C)	Est (95% CI)	0.59 (0.39, 0.76)	0.79 (0.60, 0.92)
		P-value	0.46	<0.01
	Consensus (excl. rater D)	Est (95% CI)	0.55 (0.36, 0.74)	0.90 (0.73, 0.98)
		P-value	0.71	<0.01
MRI	A	Est (95% CI)	0.62 (0.42, 0.79)	0.66 (0.46, 0.82)
		P-value	0.26	0.14
	B	Est (95% CI)	0.55 (0.36, 0.74)	0.66 (0.46, 0.82)
		P-value	0.71	0.14
	C	Est (95% CI)	0.55 (0.36, 0.74)	0.90 (0.73, 0.98)
		P-value	0.71	<0.01
	D	Est (95% CI)	0.93 (0.77, 0.99)	0.14 (0.04, 0.32)
		P-value	<0.01	<0.01
	Consensus	**Est (95% CI)**	**0.59 (0.39, 0.76)**	**0.83 (0.64, 0.94)**
		P-value	**0.46**	**<0.01**
	Consensus (excl. rater A)	Est (95% CI)	0.62 (0.42, 0.79)	0.62 (0.42, 0.79)
		P-value	0.26	0.26
	Consensus (excl. rater B)	Est (95% CI)	0.72 (0.53, 0.87)	0.66 (0.46, 0.82)
		P-value	0.02	0.14
	Consensus (excl. rater C)	Est (95% CI)	0.72 (0.53, 0.87)	0.45 (0.26, 0.64)
		P-value	0.02	0.71
	Consensus (excl. rater D)	Est (95% CI)	0.55 (0.36, 0.74)	0.83 (0.64, 0.94)
		P-value	0.71	<0.01

Table 2. Sensitivity and specificity values for individual raters, consensus as a group and with remove-one analysis completed for each rater.

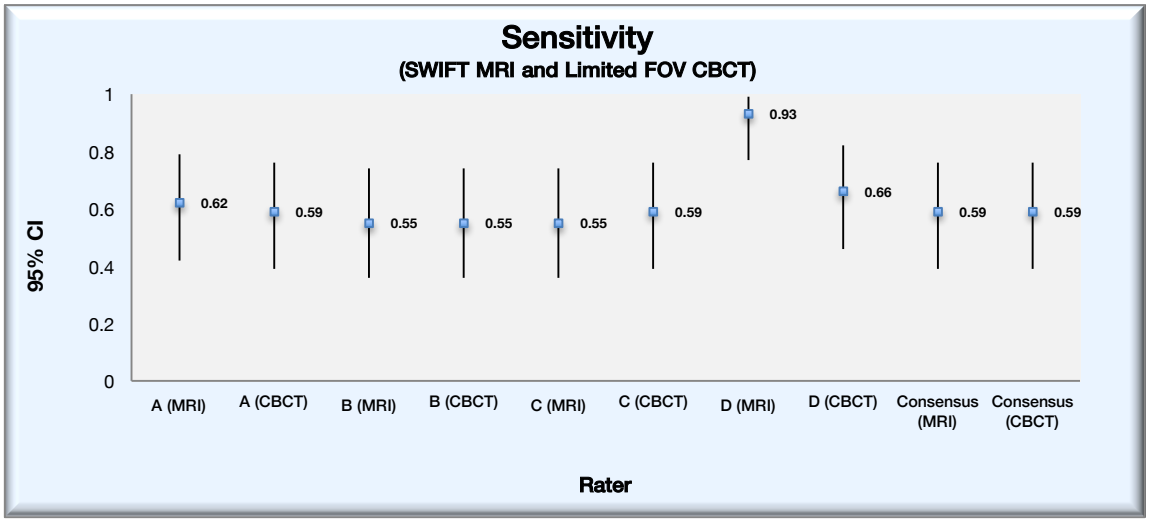

Figure 14. Individual rater and consensus sensitivity values for MRI and CBCT.

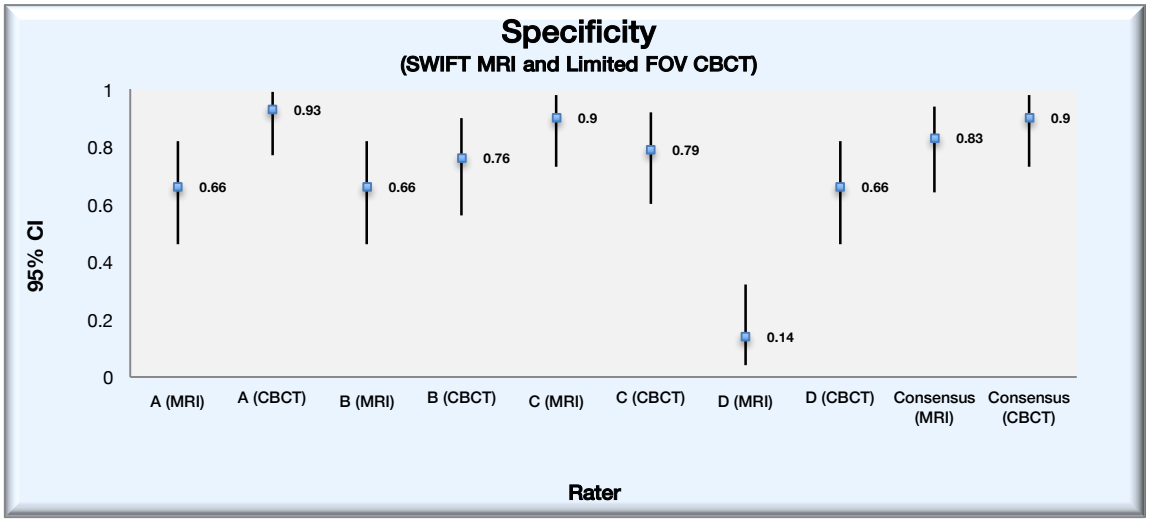

Figure 15. Individual rater and consensus specificity values for MRI and CBCT.

Intra-rater reliability for MRI was fair-to-almost perfect ($\varkappa$=0.38-1.00) and for CBCT was moderate-to-almost perfect ($\varkappa$=0.66-1.00) (**Table 3**).

Measurement	Rater	Kappa	95% CI	P-value
CBCT	A	1.00 (perfect)	(1.00, 1.00)	0.0005
	B	0.80 (almost perfect)	(0.43, 1.00)	0.0047
	C	0.80 (almost perfect)	(0.43, 1.00)	0.0047
	D	0.66 (substantial)	(0.22, 1.00)	0.0228
MRI	A	0.50 (moderate)	(0.08, 0.92)	0.0455
	B	0.38 (fair)	(-0.004, 0.77)	0.0910
	C	0.82 (almost perfect)	(0.50, 1.00)	0.0038
	D	1.00*	NA	NA

Table 3. Intra-rater agreement. Kappa statistics and its 95% confidence interval are reported. P-value is calculated for testing Kappa=0. Kappa <0.00 is poor; 0.00-0.20 slight; 0.21-0.40 fair; 0.41-0.60 moderate; 0.61-0.80 substantial; 0.81-1.00 almost perfect. * – *Kappa formula is not calculable, as 0 in numerator = undefined. However, 1.0 + undefined = 1.0*

Overall, there was non-substantial (κ<0.61) (94) inter-rater agreement for the two diagnostic imaging modalities evaluated in the study, with MRI demonstrating fair agreement (κ=0.21; 95%CI:0.10-0.31; p< 0.001) and CBCT moderate agreement (κ=0.45; 95%CI:0.34-0.56; p<0.001) (**Table 4a-e, Figure 16**).

Table 4a. All Raters			
Measurement	Kappa	95% CI	P-value
CBCT	0.45 (moderate)	(0.34, 0.56)	<.0001
MRI	0.21 (fair)	(0.10, 0.31)	<.0001

Table 4b: Excluding Rater A			
Measurement	Kappa	95% CI	P-value
CBCT	0.39 (fair)	(0.24, 0.54)	<.0001
MRI	0.11 (slight)	(-.03, 0.26))	0.0651

Table 4c: Excluding Rater B			
Measurement	Kappa	95% CI	P-value
CBCT	0.43 (moderate)	(0.28, 0.58)	<.0001
MRI	0.16 (slight)	(0.01, 0.30)	0.0196

Table 4d: Excluding Rater C			
Measurement	Kappa	95% CI	P-value
CBCT	0.48 (moderate)	(0.33, 0.63)	<.0001
MRI	0.11 (slight)	(-.04, 0.26)	0.0794

Table 4e: Excluding Rater D			
Measurement	Kappa	95% CI	P-value
CBCT	0.51 (moderate)	(0.36, 0.66)	<.0001
MRI	0.39 (fair)	(0.24, 0.53)	<.0001

Table 4a-e. Inter-rater agreement. SAS macro % agree was used to calculate inter-rater agreement. Kappa statistics and its 95% confidence interval are reported. P-value was calculated for testing Kappa=0.

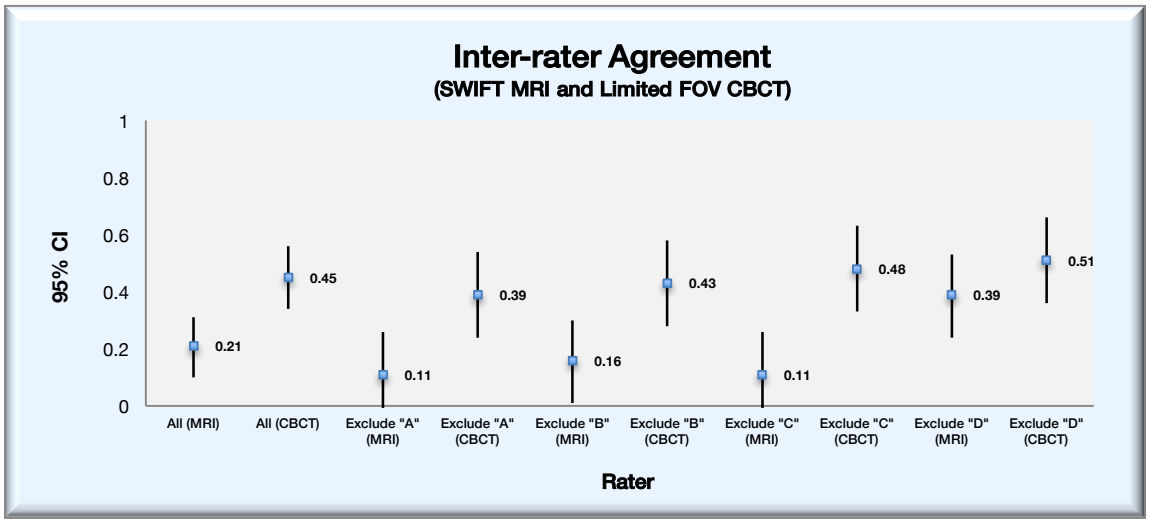

Figure 16. Inter-rater agreement. SAS macro % agree was used to calculate inter-rater agreement. Kappa statistics and its 95% confidence interval are reported. P-value was calculated for testing Kappa=0.

Experimental Study

Qualitative Results

As an exploratory outcome, each rater was asked what 10 image-sets best demonstrated the ability for SWIFT MRI to detect radicular cracks and fractures. The top 4 most-named images sets (i.e. teeth) were then selected (**Figures 17-20**). Rater's free-response comments were unanimous, selecting these images due to decreased presence or absence of artifacts associated with radio-dense filling materials and/or beam hardening artifacts. Therefore, these select image sets (**Figures 17-20**) represent the four best-case scenarios for detection of radicular cracks and fractures in the experimental image modality explored in this study (SWIFT MRI).

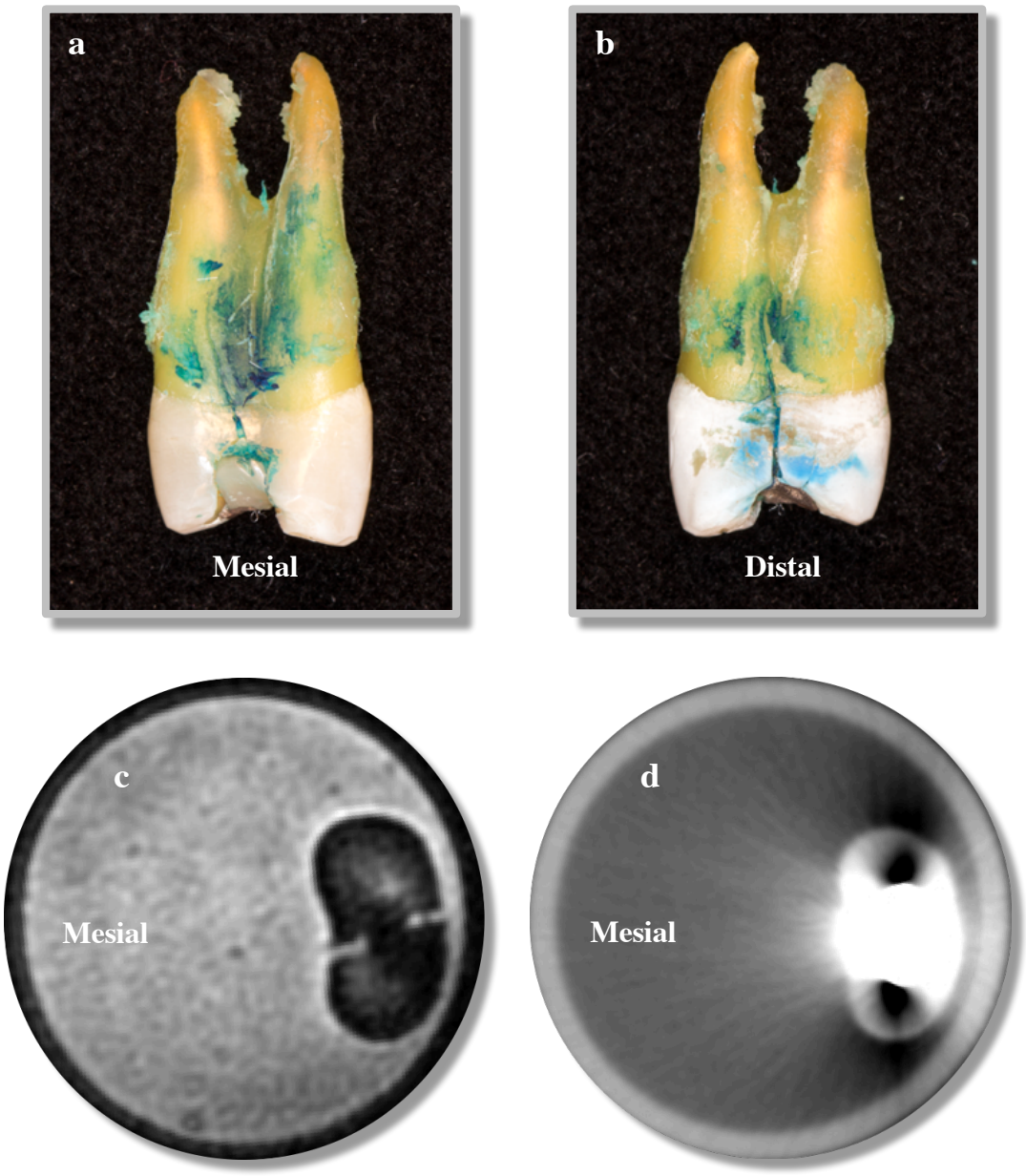

Figure 17a-e. Maxillary 1st premolar with mesial and distal cracks. Selected corresponding axial slices: SWIFT MRI (c) with notable absence of metal streak artifact from amalgam core restoration, and limited FOV CBCT (d) with severe metal streak and beam-hardening artifacts.

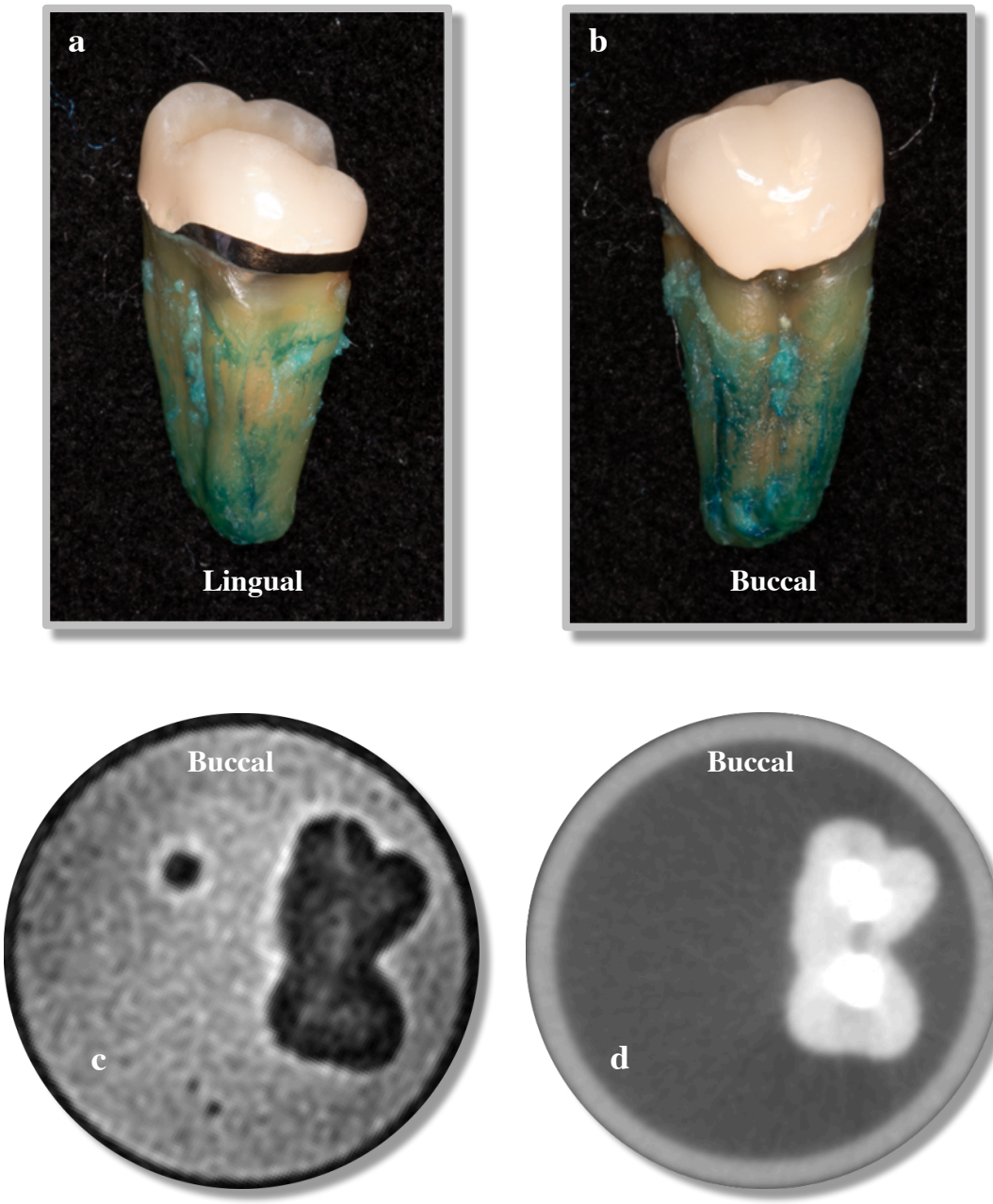

Figure 18a-e. Maxillary 2nd molar with VRF progressing from lingual to buccal root surfaces. Selected corresponding axial slices: SWIFT MRI (c) with notable absence of artifact from radio-dense root filling materials, and limited FOV CBCT (d) with moderate, radio-dense root filling material-associated artifacts and beam-hardening artifacts.

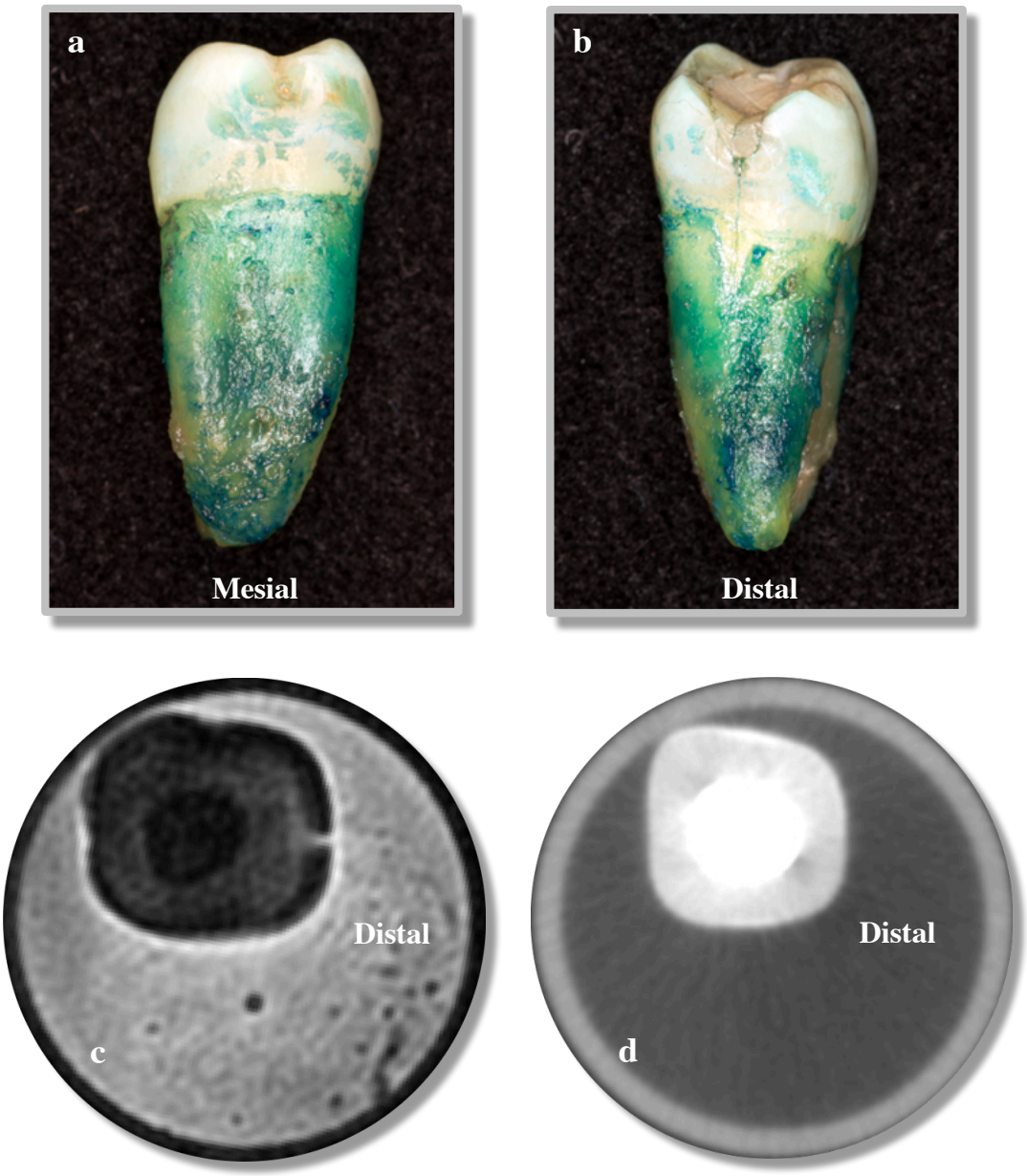

Figure 19a-e. Mandibular 1st molar with a distal crack. Selected corresponding axial slices: SWIFT MRI (c) with notable absence of metal streak artifact from amalgam core, and limited FOV CBCT (d) with severe metal streak and beam-hardening artifacts.

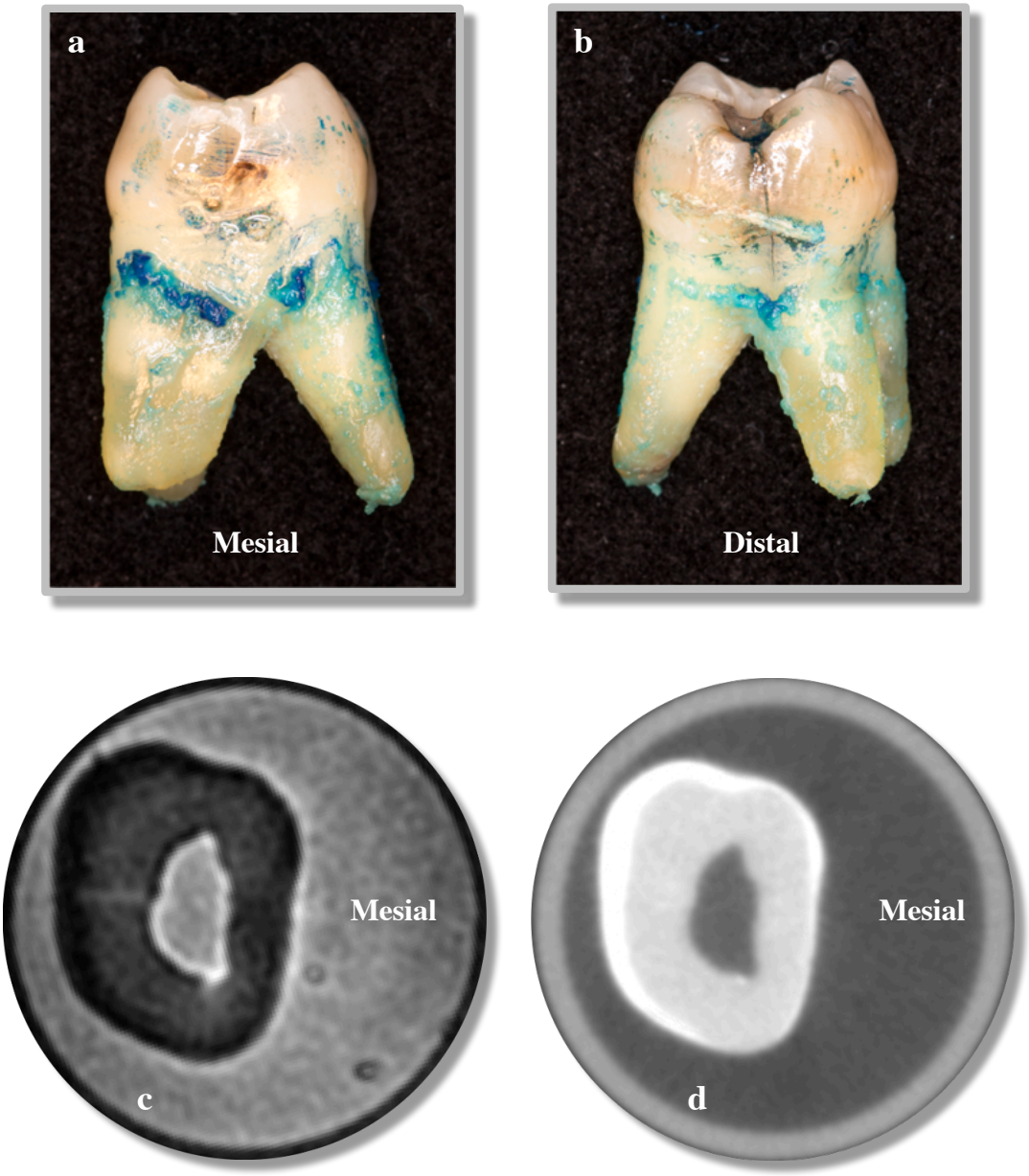

Figure 20a-e. Maxillary 1st molar with a distal crack. Selected corresponding axial slices: SWIFT MRI (c) with a high-contrast appearance of the distal crack, and limited FOV CBCT (d) with low-contrast appearance of the same distal crack.

DISCUSSION

One of the specific aims of this *ex vivo* study was to characterize the visual representations of tooth-root cracks/fractures in MR imaging. These visual features were utilized in the development of a novel MRI-based criteria for crack/fracture appearance within this alternate 3D imaging modality. In fulfilling this specific aim, future experimental research in this area can employ and further refine this criteria. At the time of thesis publication, no prior studies have outlined MRI-based criteria for discontinuities in tooth structure. Also of importance – ***Specific Aim 2 and 3*** of the study – investigating the feasibility of the SWIFT MRI scans in detecting radicular cracks/fractures, by way of comparing rater reliabilities and corresponding sensitivity and specificity values to the current clinical standard, limited FOV CBCT (4). Tooth cracks/fractures have been an area of collective importance for several decades due to an increased prevalence associated with advancing patient age and improved clinical awareness by the treating clinician (51). Improvements in lifetime tooth retention have led to a growth in the number of patients presenting with a lengthier cumulative history of complex restorative, prosthetic and endodontic procedures that may pre-dispose the aging dentition to higher crack/fracture susceptibility (25,26). These physical discontinuities in radicular tooth structure allow ingress of oral irritants, such as salivary components, bacteria and chemical substances (100). Left unchecked, the persistence of crack/fracture biofilms may facilitate radicular pathosis that is recalcitrant to root canal treatment (38,39), likely resulting in progressive destruction of the periodontium (41).

The clinical significance of tooth-root cracks and fractures is centered on those discontinuities that cannot be visualized definitively in the absence of invasive measures such as X-ray-based 3D CBCT imaging, direct visualization via non-surgical endodontic access or surgical flap reflection (7,8). Therefore, clinical dentistry is in need of a non-invasive, efficient and accurate diagnostic method to better evaluate radicular fracture pathosis in attempts to establish a more predictable dental prognosis. The AAE has clearly made cracked tooth studies a top research priority (65), recently publishing guidelines for methodology to aid institutions, practice-based research networks and

practitioners in developing meaningful studies to appropriately gauge incidence and prevalence of root cracks or fractures in teeth (5). Other emerging diagnostic modalities such as Near-Infrared Range (NIR), Ultrasound, and Optical Coherence Tomography (OCT) are more directly applicable to identifying those discontinuities that are located in supra-gingival dental tissues and thus, have produced varying results in radicular crack/fracture detection (80–83).

The results of the present study suggest education and training for both MR and CBCT imaging modalities is needed to improve reliabilities for the identification of tooth-root crack(s)/fracture(s). Irrespective of 3D imaging techniques used in the present study, inter-rater agreement was non-substantial ($\varkappa < 0.61$) (94). Similarities between MRI and CBCT accuracy were also observed, with comparatively high specificity (0.83 and 0.90, respectively) and poor sensitivity (0.59 and 0.59, respectively). Despite the advantages of increased contrast (19) and absence of artifact from radio-dense filling materials in MR imaging (86), comparable measures of sensitivity and specificity (with respect to CBCT) suggest MRI quality improvements are needed, specifically in image acquisition and post-processing parameters.

Nearly half of the teeth (45%) included in the study contained root canal filling materials. Though, the influence of root canal filling material presence on rater-reliability or accuracy of crack/fracture detection in MRI and CBCT was not specifically evaluated in this research. Prior *ex vivo* studies have evaluated this potential affect in CBCT (93,98), noting decreases in specificity but with no significant decrease in overall accuracy. Dental CBCT has had periodic technological improvements that now allow smaller FOV, providing increased resolution while decreasing scan time and corresponding radiation dose (75). Aside from the presence of ionizing radiation, the potential for significant CBCT image artifact associated with coronal and radicular radio-dense dental materials remains one of the primary shortcomings of this 3D image modality when attempting to evaluate neighboring structures – especially with larger FOV sizes (74,75). Interestingly, image artifacts from gold or amalgam restorations are notably absent in MRI (86). That finding was clearly demonstrated on multiple occasions in this study – including a near complete absence of radio-dense, material-associated

artifact when examining previously root-filled teeth that contained gutta-percha and endodontic sealer (**Figures 17-20**). This obvious advantage demonstrates the potential power of the SWIFT MRI technique in aiding tooth-root crack/fracture detection in commonly encountered clinical situations that involve previously root-filled teeth.

In the present study, the inherent advantages of increased contrast (19) and absence of artifact from radio-dense filling materials in MR imaging (86) appeared to be countered in part by MR imaging error. This may be attributed to several factors that are likely related to image acquisition and image optimization parameters; currently no proprietary, commercially available, dental-specific MR image reconstruction software program exists to manage the projection data for construction of a 3D volumetric data set. Throughout the calibration and experimental study, projection data reconstruction was completed solely by an MRI physicist [DI] and a board-certified OMF radiologist [LG].

The major identified sources of dental-specific, MR-associated imaging error in the present study involve image focus and loss of image signal. Perhaps the largest of these errors lies in image focusing problems observed in the study. The resulting SWIFT MR images had a variable focus, meaning within the stack of axial DICOM image slices, differences between in-, and-out-of-focus images within each MR image set were observed. This focus issue was reflected in the language used to develop the MRI-based criteria for cracks/fractures: *"1 or 2 usually sharply defined, high-signal (bright or white) line shapes, presenting as single entities, or parallel pairs in close proximity, or pairs in close proximity exhibiting convergence or divergence…"*. The *"1 or 2…line shapes"* described highlight the variable presentation of cracks/fractures (**Figure 13**). A blinded operator [DN], unaware of crack/fracture status, made a subjective determination of the single image focus plane that resulted in the overall, best focus for the radicular axial slices. This variable focus issue was identified as a significant shortcoming of the study. Improvements via software enhancements, such as auto-refocusing or user-adjusted focusing, could allow rater-review of in-focus images like that of proprietary CBCT software packages.

Additionally, image drop-out or loss of image signal at the tooth apex was an often-reported rater issue in a post-study survey. Put simply, the signal to noise ratio

(SNR) is equal to the ratio of the average signal intensity over the standard deviation of noise (99). SNR is dependent on many parameters, however the observed image drop-out in this study was primarily due to the lack of homogenous signal intensity across the entire axial image stack. This graduated decrease in image value or brightness was due to physical limitations of the custom-built RF coil. The details of RF coil physics are complicated and thus beyond the scope of this paper. Following the study, researchers at UMN's CMRR developed a new, custom-built RF intraoral apparatus for use in future research; improvements made to the earlier single-coil design include 3 additional coils, 1 external to each cheek and 1 facial to the anterior dentition, to decrease loss of signal intensity at the tooth apex (**Figure 21 – *see Appendix VII***)

Outside of image acquisition and software enhancements, the preparation of DICOM axial image stacks for both imaging modalities could be improved. To restrict the raters' review to radicular-only axial image slices for crack/fracture, the primary anatomic focus of the study, we elected to digitally crop the image to remove the crown. Every attempt was made to crop each tooth image set at the same location as outlined in the study design. However, we understand the limitations with this method as the cemento-enamel junction (CEJ) has both horizontal and vertical orientations that are not amenable to a strictly linear image cropping technique (**Figure 11a,c**). Tooth-root position within each glass vial was made near-vertical to the outside vial wall. Though, inconsistency in this positioning, as well as positioning in the scanners, may have contributed to an increase in variability within this digital cropping technique (**Figure 11c**). If the tooth was positioned off-angle, linear cropping would result in potential absence of several axial image slices that contain radicular tooth structure, perhaps excluding known ground truth coronally position cracks from the experimental axial slice image sets (**Figure 11b**). Post-processing could be improved in future research by utilizing an image-editing software package that allows vertical tooth position changes and non-linear digital image cropping.

The present study was designed to include an *ex vivo* tooth sample previously diagnosed by an experienced board-certified endodontist [AL] as having a non-restorable crack/fracture. We included these clinical-based samples with naturally occurring

cracks/fractures to aid in the development of an MRI-based criteria that would best represent what would be encountered clinically by diagnosticians. As a byproduct of obtaining such a sample, the study was slightly underpowered. Completion of the study with a larger convenience sample or directing future research to an artificially-induced crack/fracture model would allow higher sample sizes and the ability to explore other possible aims such as crack/fracture width or extent and the effect on MR imaging.

Each MR image acquisition was completed with 10 teeth/scan, 5 teeth positioned superior, and 5 teeth inferior to RF coil due to space limitations encountered during mounting of the *ex vivo* sample in glass vials (**Figures 10a-c**). The smallest available vials that would accommodate a single human tooth were utilized to maintain tooth position, reduce tooth movement, and to maintain constant tooth moisture content that would best simulate the natural moisture in an oral cavity throughout the *ex vivo* scanning process.

Limited FOV CBCT imaging was accomplished with 1 tooth/scan to reduce the potential for any confounding artifacts from radio-dense filling materials that would degrade image quality of the individual teeth during evaluation. Acquiring limited FOV CBCT images (at 0.076mm isotropic voxel size) in this fashion could be perceived as a limitation as it is not indicative of a typical clinical situation, and would thus produce near-mythical, and clinically-unattainable image quality with little noise. However, this was done purposefully to exclude possible metal streak artifact from a neighboring tooth and to serve both as an early, and intentionally challenging initial comparison test for the SWIFT MRI technique in tooth-root crack/fracture detection. Interestingly, despite this clinically unachievable and perhaps unrealistic CBCT image quality, the inter-rater reliability for limited FOV CBCT (κ=0.45; 95%CI:0.34-0.56; $p<0.001$) was only marginally better than SWIFT MRI (κ=0.21; 95%CI:0.10-0.31; $p< 0.001$); both 3D image modalities demonstrated non-substantial agreement ($\kappa< 0.61$) (94).

The CBCT inter-rater agreement presented here was slightly higher than a 2014 *ex vivo* study (κ=0.45 vs. κ= 0.33, respectively) that investigated a similar limited FOV CBCT unit by evaluating artificially induced, incomplete VRFs (17). However, that study evaluated both incomplete and complete VRFs, a designation that was not differentiated

in the present study. The specificity of CBCT in crack/fracture detection demonstrated in this study (0.90) was similar to a 2009 ex vivo study involving artificially induced VRFs (0.93), (98) though sensitivity in the same study (0.79) was noticeably higher than noted in the present research (0.59). A 2011 clinically-based CBCT study (16) reported a higher sensitivity value (0.88 to 0.59), but a lower specificity value (0.75 to 0.90) when compared to this *ex vivo* study. These differences in reported CBCT sensitivities and specificities may be due to the variability in crack/fracture extent or completeness, which was not a measured outcome in this study.

Similarities in accuracy and reliability among the two image modalities may be due to the types of fractures examined in this study. The experimental teeth were extracted after declaration of non-restorability following diagnosis of cracked tooth or VRF by an experienced, board-certified endodontist. It could be inferred that teeth designated for extraction due to diagnosis of crack/fracture would be expected to have an increased extent of physical discontinuity, that if true, may have nullified the enhanced resolving power of MRI noted in earlier research (19). The failure to measure the extent or width of crack(s)/fracture(s) may be seen as a shortcoming of the study. Future studies could be improved by incorporating MicroCT imaging as an accepted gold standard to assess both the presence and extent of cracks and/or fractures in the calibration sample (44). MicroCT imaging was not included in the present study due to limitations in laboratory funding and time constraints with the labor-intensive image reconstruction. If the understanding of crack/fracture width and/or extent as it relates to both visualization and image interpretation could be enhanced, a further optimized SWIFT MR imaging technique could conceivably be utilized as a novel diagnostic screening aid in the detection of early, asymptomatic radicular cracks/fractures. Identifying these discontinuities sooner could allow for more conservative, restorative-based treatments that may prevent the need for future dental extraction.

Development of a new 3D imaging technology for dental applications is not without cost. One potential shortcoming of the utilization of MRI for dental-based applications involves reduced clinical acceptance due to cost-associated factors and physical space limitations. As a result, current medical-based MR systems are typically

limited to hospitals and major out-patient trauma centers. This could be seen as a barrier to further MRI development for dental-specific applications. However, one may realize the potential for future developments of dental-specific 3D imaging modalities by examining the historical developments of computed tomography (CT) in medicine and CBCT in dentistry.

The early advancement of CBCT technology in the 1990s was primarily for the purposes of entering the dental office setting (75,101). Factors involved with the rapid incorporation of CBCT for dentistry include the availability of improved, rapid, and cost-effective computer technology and the ability of software engineers to develop multiple dental imaging applications for CBCT with broad diagnostic capability (75). The physical size and shape of CBCT closely mirrored the path of panoramic imaging development (supine (102), to sit-down (103,104), to standing), standing being more preferable due to ease of patient transferal. In early CBCT development the FOV was fixed, with unit cost and size proportional to FOV size. Larger FOV sizes were limited in application and subjected the patient to higher radiation dosages, therefore exploration of smaller FOV sizes lead to the development of reduced CBCT scanner sizes (75).

Smaller, more compact MRI scanning systems have already been developed. In 2016 the Mayo Clinic unveiled a new, one-of-a-kind, compact 3T MRI scanner designed by General Electric (GE) in collaboration with a National Institutes of Health (NIH) Bioengineering Research Partnership between GE's Global Research Center and Mayo Clinic. This new prototype magnet was designed for scanning of the head and smaller extremities and is therefore approximately one-third the size of conventional systems (105). The reduced scanner size allows for easier installation in space-constrained locations, a smaller electrical footprint that reduces scan times, and improved patient comfort.

Regardless of the current MR unit size, several benefits exist that may warrant future use and development for specific dental applications. The benefits may include – but are not limited to – simultaneous, non-ionizing imaging of soft and calcified dental tissues with larger attainable FOV dimensions, without the fears of increased radiation exposure that exist in X-ray-based imaging modalities such as CBCT. Prior *in vivo*

research utilizing the custom-built intraoral RF coil used in this study has demonstrated the ability of SWIFT MRI to capture larger fields of view, including an entire natural adult dentition in a single 3.5-minute scan, free of metal streak artifact with many common non-ferrous dental materials (19). This is in contrast to CBCT radiographic imaging; larger FOV sizes generally lead to poorer image quality due to noise from large amounts of scattered ionizing radiation, increased presence of beam hardening and metal artifact (106).

Despite current limitations and the early stage of technological development, the benefits offered, including: multiple available pathways to optimize MR imaging of teeth, absence of ionizing radiation, and the inherent advantages of increased contrast and absence of artifact from radio-dense materials – suggest there may be a use for SWIFT MRI in detecting cracks and fractures in teeth.

Future Areas of Study

The present research builds upon past studies and moves towards further optimization of SWIFT MRI for dental-associated applications to advance the understanding of clinically relevant dental problems such as detecting the presence of radicular cracks and fractures in teeth – the ***Specific Aims 2 and 3*** of this study. Future applications would likely involve evaluating the minimum physical size of clinically relevant cracks/fractures that permits detection using the SWIFT MRI. If smaller cracks/fractures are able to be diagnosed with MRI, then it is conceivable that future in vivo studies could provide earlier detection, thus allowing avenues for employment of preventative restorative and prosthetic measures to halt crack propagation and the potential need for dental extraction. Future areas of MR-based dental research could also be devoted to dento-alveolar trauma cases to aid in the detection of trauma-based cracks and fractures in teeth. With minimal dental material associate-artifact and the ability to utilize dental MRI at clinically relevant scan times (e.g. 3.5 minutes), the increased FOV size could permit scanning of the entire dentition in a single scan at a hospital or trauma center – without the use of ionizing radiation. Additionally, the advantages of

simultaneous, 3D soft and hard-tissue visualization with MRI may allow both crack/fracture detection as well as assessment of pulpal blood flow in the potential determination of tooth vitality. Further image optimization enhancements and clinically-based research studies involving MRI for dental applications may permit wider acceptance of this 3D imaging modality. With approval from the dental community, MR-based technological advancements could allow future, in-office use of this non-ionizing 3D imaging modality.

CONCLUSION

Education and training for both CBCT and MR imaging modalities is needed to improve reliabilities for the identification of tooth-root crack/fractures. Despite the advantages of increased contrast and absence of artifact from radio-dense materials in MRI, comparable measures of sensitivity and specificity (in relation to CBCT) suggest quality MRI improvements are needed, specifically in image acquisition and post-processing parameters. Given the early stage of technology development and multiple available pathways to optimize MR imaging of teeth, there may be a use for SWIFT MRI in detecting cracks and fractures in teeth.

Bibliography

1 Cohen Stephen, Blanco Lucia, Berman Louis. Vertical root fractures Clinical and radiographic diagnosis. J Am Assoc 2003;134(4):434–41.

2 Stanley Harold R. The Cracked Tooth Syndrome. J Am Acad Gold Foil Oper 1968;11:36–47.

3 Berman Louis H, Hartwell Gary R. Diagnosis. *Cohen S, Hargreaves KM, eds. Pathways Pulp. St. Louis Mosby Elsevier*. Elsevier Health Sciences; 2011. p. 24–31.

4 Rivera Eric, Walton E Richard. Cracking The Cracked Tooth Code: Detection and Treatment of Various Longitudinal Tooth Fractures. Endod Colleagues Excell 2008;Summer:2–7.

5 Friedman Shimon, Azarpazhooh Amir, Bruder George A, et al. Guidelines for the Methodology of Cracked Tooth Studies. Am Assoc Endodontists 2016:www.aae.org.

6 Scarfe WC, Farman a G, Sukovic P. Clinical applications of cone-beam computed tomography in dental practice. J Can Dent Assoc 2006;72(1):75–80.

7 Lommell Tennyson J, Meister Frank, Gerstein Harold, Davies E Esch, Tilk Mary Ann. Alveolar bone loss associated with vertical root fractures. Oral Surg 1978;45:909–18.

8 Pitts David L, Natkin Eugene. Diagnosis and treatment of vertical root fractures. J Endod 1983;9(8):338–46. Doi: 10.1016/S0099-2399(83)80150-2.

9 Moule a J, Kahler B. Diagnosis and management of teeth with vertical root fractures. Aust Dent J 1999;44(2):75–87. Doi: 10.1016/S0099-2399(83)80150-2.

10 Ingle JL. *Endodontics*. Philadelphia: Lea & Febiger; 1972.

11 Tamse a, Fuss Z, Lustig J, Ganor Y, Kaffe I. Radiographic features of vertically fractured, endodontically treated maxillary premolars. Oral Surg Oral Med Oral Pathol Oral Radiol Endod 1999;88(3):348–52. Doi: S1079-2104(99)70041-7 [pii].

12 Shemesh Hagay, van Soest Gijs, Wu Min Kai, Wesselink Paul R. Diagnosis of Vertical Root Fractures with Optical Coherence Tomography. J Endod

2008;34(6):739–42. Doi: 10.1016/j.joen.2008.03.013.

13 Special Committee to Revise the Joint AAE/AAOMR Position Statement on use of CBCT in Endodontics. AAE and AAOMR Joint Position Statement: Use of Cone Beam Computed Tomography in Endodontics 2015 Update. Oral Surg Oral Med Oral Pathol Oral Radiol 2015;120(4):508–12. Doi: 10.1016/j.oooo.2015.07.033.

14 Liedke Gabriela Salatino, da Silveira Heloísa Emília Dias, da Silveira Heraldo Luis Dias, Dutra Vinícius, de Figueiredo José Antônio Poli. Influence of Voxel Size in the Diagnostic Ability of Cone Beam Tomography to Evaluate Simulated External Root Resorption. J Endod 2009;35(2):233–5. Doi: 10.1016/j.joen.2008.11.005.

15 Beam Cone, Tomography Computed. AAE and AAOMR Joint Position Statement. J Endod 2015;41(9):1393–6. Doi: 10.1016/j.joen.2015.07.013.

16 Edlund Mitchell, Nair Madhu K, Nair Umadevi P. Detection of vertical root fractures by using cone-beam computed tomography: A clinical study. J Endod 2011;37(6):768–72. Doi: 10.1016/j.joen.2011.02.034.

17 Brady E, Mannocci F, Brown J, Wilson R, Patel S. A comparison of cone beam computed tomography and periapical radiography for the detection of vertical root fractures in nonendodontically treated teeth. Int Endod J 2014;47(8):735–46. Doi: 10.1111/iej.12209.

18 Setzer Frank C, Hinckley Nathan, Kohli Meetu R, Karabucak Bekir. A Survey of Cone-beam Computed Tomographic Use among Endodontic Practitioners in the United States. J Endod 2017;43(5):699–704. Doi: 10.1016/j.joen.2016.12.021.

19 Idiyatullin Djaudat, Corum Curt, Moeller Steen, Prasad Hari S, Garwood Michael, Nixdorf Donald R. Dental magnetic resonance imaging: Making the invisible visible. J Endod 2011;37(6):745–52. Doi: 10.1016/j.joen.2011.02.022.

20 Gonzalez Ballester Miguel Angel, Zisserman Andrew P, Brady Michael. Estimation of the partial volume effect in MRI. Med Image Anal 2002;6(4):389–405. Doi: 10.1016/S1361-8415(02)00061-0.

21 Idiyatullin Djaudat, Corum Curt, Park Jang Yeon, Garwood Michael. Fast and quiet MRI using a swept radiofrequency. J Magn Reson 2006;181(2):342–9. Doi:

10.1016/j.jmr.2006.05.014.

22 Pasteris Jill D, Wopenka Brigitte, Valsami-Jones Eugenia. Bone and tooth mineralization: Why apatite? Elements 2008;4(2):97–104. Doi: 10.2113/GSELEMENTS.4.2.97.

23 Ellis SG, McCord JF, Burke FJ. Predisposing and contributing factors for complete and incomplete tooth fractures. Dent Update 1999;26(4):150–2, 156–8.

24 Braly B V., Maxwell EH. Potential for tooth fracture in restorative dentistry. J Prosthet Dent 1981;45(4):411–4. Doi: 10.1016/0022-3913(81)90102-5.

25 Homewood CI. Cracked tooth syndrome--incidence, clinical findings and treatment. Aust Dent J 1998;43(4):217–22.

26 Cameron Caryl E. The cracked-tooth syndrome: additional findings. J Am Dent Assoc 1976;93:971–5.

27 Gross A, Rivera-Morales W, Gale E. A prevalence study of symptoms associated with TM disorders. J Craniomandib Disord Facial Oral Pain 1988;2(4):191–5.

28 Egermark-Eriksson I, Carlsson GE, Ingervall B. Prevalence of mandibular dysfunction and orofacial parafunction in 7-, 11- and 15-year-old Swedish children. Eur J Orthod 1981;3:163–72.

29 Allen JD, Rivera-Morales WC, Zwemer JD. Occurrence of temporomandibular disorder symptoms in healthy young adults with and without evidence of bruxism. Cranio 1990;8(4):312–8.

30 Okeson JP, Phillips BA, Berry DTR, Cook Y, Paesani D, Galante J. Nocturnal bruxing events in healthy geriatric subjects. J Oral Rehabil 1990;17(5):411–8. Doi: 10.1111/j.1365-2842.1990.tb01412.x.

31 Okeson JP, Phillips BA, Berry DT, Cook YR, Cabelka JF. Nocturnal bruxing events in subjects with sleep-disordered breathing and control subjects. J Craniomandib Disord 1991;5(4):258–64.

32 Okeson JP, Phillips BA, Berry DT, Baldwin RM. Nocturnal bruxing events: a report of normative data and cardiovascular response. J Oral Rehabil 1994;21(6):623–30. Doi: 10.1111/j.1365-2842.1994.tb01177.x.

33 Pavone BW. Bruxism and its effect on the natural teeth. J Prosthet Dent 1985. Doi:

http://dx.doi.org/10.1016/0022-3913(85)90026-5.

34 Rivera EM, Williamson A. Diagnosis and treatment planning: cracked tooth. Tex Dent J 2003;120(278–283):38–41.

35 Rivera Eric M, Walton Richard E. Longitudinal tooth fractures: findings that contribute to complex endodontic diagnoses. Endod Top 2009;16(1):82–111. Doi: 10.1111/j.1601-1546.2009.00243.x.

36 Tamse Aviad. Iatrogenic vertical root fractures in endodontically treated teeth. Dent Traumatol 1988:190–6. Doi: 10.1111/j.1600-9657.1988.tb00321.x.

37 Goldman Melvin, Pear. Endodontic success - Who's reading the radiograph 1972.

38 Kahler Bill, Moule Alex, Stenzel Deb. Bacterial contamination of cracks in symptomatic vital teeth. Aust Endod J 2000;26(3):115–8. Doi: 10.1111/j.1747-4477.2000.tb00296.x.

39 Ricucci Domenico, Siqueira José F, Loghin Simona, Berman Louis H. The cracked tooth: Histopathologic and histobacteriologic aspects. J Endod 2015;41(3):343–52. Doi: 10.1016/j.joen.2014.09.021.

40 Tan L, Chen NN, Poon CY, Wong HB. Survival of root filled cracked teeth in a tertiary institution. Int Endod J 2006;39(11):886–9. Doi: 10.1111/j.1365-2591.2006.01165.x.

41 Hiatt WH. Incomplete crown-root fracture in pulpal-periodontal disease. J Periodontol 1973;44(6):369–79. Doi: 10.1902/jop.1973.44.6.369.

42 Kang Sung Hyun, Kim Bom Sahn, Kim Yemi. Cracked teeth: Distribution, characteristics, and survival after root canal treatment. J Endod 2016;42(4):557–62. Doi: 10.1016/j.joen.2016.01.014.

43 Turp Jens C, Gobetti John P. The Cracked Tooth Syndrome: An Elusive Diagnosis. J Am Dent Assoc 1996;127(10):1502–7. Doi: 10.14219/jada.archive.1996.0060.

44 Berman Louis H, Kuttler Sergio. Fracture Necrosis: Diagnosis, Prognosis Assessment, and Treatment Recommendations. J Endod 2010;36(3):442–6. Doi: 10.1016/j.joen.2009.12.018.

45 Evans Philip M. Anatomical imaging for radiotherapy. Phys Med Biol

2008;53(12):R151–91. Doi: 10.1088/0031-9155/53/12/R01.

46 Lagouvardos P, Sourai P, Douvitsas G. Coronal fractures in posterior teeth. Oper Dent 1989;14(1):28–32.

47 Talim ST, Gohil KS. Management of coronal fractures of permanent posterior teeth. J Prosthet Dent 1974;31(2):172–8. Doi: 10.1016/0022-3913(74)90052-3.

48 Sugaya T, Kawanami M, Noguchi H, Kato H, Masaka N. Periodontal healing after bonding treatment of vertical root fracture. Dent Traumatol 2001;17(4):174–9. Doi: 10.1034/j.1600-9657.2001.170407.x.

49 Dederich Douglas N, Sc M, Ph D. Case Report Co 2 Laser Fusion of a Vertical Root Fracture 2001;130(August 1999):1195–9.

50 Walton Richard E, Torabinejad Mahmoud. Cracked tooth and vertical root fracture. *Princ. Pract. Endod*. 2nd ed. 1996. p. 474–92.

51 Endodontists American Association of. Cracking THe Cracked Tooth Code. Endod Colleagues Excell 1997;Fall/Winte:1–8.

52 Walton Richard E, Rivera Eric M. Longitudinal tooth fractures. *Princ. Pract. Endod*. 3rd ed. Saunders Company; 2002. p. 474–92.

53 Rivera Eric M, Walton Richard E. Longitudinal tooth fractures. *Princ. Pract. Endod*. 3rd ed. Philadelphia, PA: W. B. Saunders Company; 2009. p. 108–28.

54 Tsesis I, Tamse A, Lustig J, Kaffe I. Vertical root fractures in endodontically treated teeth part I: clinical and radiographic diagnosis. Endod Top 2006;23(1):13–7, 68. Doi: 10.1111/j.1601-1546.2006.00200.x.

55 Gher ME, Dunlap RM, Anderson MH, Kuhl L V. Clinical survey of fractured teeth. J Am Dent Assoc 1987;114(2):174–7. Doi: 10.14219/jada.archive.1987.0006.

56 Patel DK, Burke FJ. Fractures of posterior teeth: a review and analysis of associated factors. Prim Dent Care 1995;2(1):6–10.

57 Meister Frank, Lommel Tennyson J, Gerstein Harold. Diagnosis and possible causes of vertical root fractures. Oral Surgery, Oral Med Oral Pathol 1980;49(3):243–53. Doi: 10.1016/0030-4220(80)90056-0.

58 Joffe E. *Management of vertical root fracture in endodontically treated teeth*. vol.

58. 1992.

59 Yang Shue Fen, Rivera Eric M, Walton Richard E. Vertical root fracture in nonendodontically treated teeth. J Endod 1995;21(6):337–9. Doi: 10.1016/S0099-2399(06)81013-7.

60 Liebow WB. The cracked tooth syndrome. Ariz Dent J 1976;22:23–6.

61 Krell Keith V., Rivera Eric M. A Six Year Evaluation of Cracked Teeth Diagnosed with Reversible Pulpitis: Treatment and Prognosis. J Endod 2007;33(12):1405–7. Doi: 10.1016/j.joen.2007.08.015.

62 Ratcliff Steve, Becker Irwin M, Quinn Linda. Type and incidence of cracks in posterior teeth. J Prosthet Dent 2001;86(2):168–72. Doi: 10.1067/mpr.2001.116578.

63 Arola D, Reprogel RK. Effects of aging on the mechanical behavior of human dentin. Biomaterials 2005;26(18):4051–61. Doi: 10.1016/j.biomaterials.2004.10.029.

64 Eakle WS, Maxwell EH, Braly B V. Fractures of posterior teeth in adults. J Am Dent Assoc 1986;112(2):215–8. Doi: 10.14219/jada.archive.1986.0344.

65 Foundation American Association of Endodontists. Endodontic Research Guidelines 2004.

66 Slaton C Cornelious, Loushine Robert J, Weller R Norman, Parker M Harry, Kimbrough W Frank, Pashley David H. Identification of resected root-end dentinal cracks: a comparative study of visual magnification. J Endod 2003;29(8):519–22. Doi: 10.1097/01.DON.0000125876.26495.20.

67 Wright Henry M, Loushine Robert J, Weller R Norman, Kimbrough W Frank, Waller Jennifer, Pashley David H. Identification of resected root-end dentinal cracks: a comparative study of transillumination and dyes. J Endod 2004;30:712–5. Doi: 10.1097/01.DON.0000125876.26495.20.

68 Tamse Aviad, Kaffe Israel, Lustig Joseph, Ganor Yehuda, Fuss Zvi. Radiographic features of vertically fractured endodontically treated mesial roots of mandibular molars. Oral Surgery, Oral Med Oral Pathol Oral Radiol Endodontology 2006;101(6):797–802. Doi: 10.1016/j.tripleo.2005.09.014.

69 Nair MK, Tyndall DA, Ludlow JB, May K. Tuned Aperture Computed Tomography and Detection of Recurrent Caries. Caries Res 1997;32(1):23–30. Doi: 10.1159/000016426.

70 Mora Maria A, Mol André, Tyndall Donald A, Rivera Eric M. In vitro assessment of local computed tomography for the detection of longitudinal tooth fractures. Oral Surgery, Oral Med Oral Pathol Oral Radiol Endodontology 2007;103(6):825–9. Doi: 10.1016/j.tripleo.2006.09.009.

71 Dowker SEP, Davis GR, Elliott JC. X-ray microtomography: Nondestructive three-dimensional imaging for in vitro endodontic studies. Oral Surg Oral Med Oral Pathol Oral Radiol Endod 1997;83(4):510–6. Doi: S1079-2104(97)90155-4 [pii].

72 White Stuart C, Pharoah MJ. No Title. *Oral Radiol. Princ. interpreatation*. 5th ed. St. Louis, MO; 2004. p. 623.

73 Fryback DG, Thornbury JR. The efficacy of diagnostic imaging. Med Decis Making 1991;11(2):88–94. Doi: 10.1177/0272989X9101100203.

74 Melo Saulo Leonardo Sousa, Bortoluzzi Eduardo Antunes, Abreu Jr. Murillo, Corr?a Let?cia Ruhland, Corr?a Marcio. Diagnostic Ability of a Cone-Beam Computed Tomography Scan to Assess Longitudinal Root Fractures in Prosthetically Treated Teeth. J Endod 2010;36(11):1879–82. Doi: 10.1016/j.joen.2010.08.025.

75 Abramovitch Kenneth, Rice Dwight D. Basic principles of cone beam computed tomography. Dent Clin North Am 2014;58(3):463–84. Doi: 10.1016/j.cden.2014.03.002.

76 Vizzotto MB, Silveira PF, Arús NA, Montagner F, Gomes BPFA, da Silveira HED. CBCT for the assessment of second mesiobuccal (MB2) canals in maxillary molar teeth: Effect of voxel size and presence of root filling. Int Endod J 2013;46(9):870–6. Doi: 10.1111/iej.12075.

77 Brynjulfsen A Grevstad T, Hals-Kvinnsland I Fristad I. Incompletely fractured teeth associated with diffuse longstandling orofacial pain: diagnosis and treatment outcome. Int Endod J 2002;35:461–6.

78 Patel S, Brady E, Wilson R, Brown J, Mannocci F. The detection of vertical root fractures in root filled teeth with periapical radiographs and CBCT scans. Int Endod J 2013;46(12):1140–52. Doi: 10.1111/iej.12109.

79 Chavda Rajesh, Mannocci Francesco, Andiappan Manoharan, Patel Shanon. Comparing the in vivo diagnostic accuracy of digital periapical radiography with cone-beam computed tomography for the detection of vertical root fracture. J Endod 2014;40(10):1524–9. Doi: 10.1016/j.joen.2014.05.011.

80 Angelino Keith, Edlund David A, Shah Pratik. Near-Infrared Imaging for Detecting Caries and Structural Deformities in Teeth 2017;5(April). Doi: 10.1109/JTEHM.2017.2695194.

81 Culjat MO, Singh RS, Brown ER, Neurgaonkar RR, Yoon DC, White Shane N. Ultrasound crack detection in a simulated human tooth. Dentomaxillofacial Radiol 2005;34(2):80–5. Doi: 10.1259/dmfr/12901010.

82 Huang D, Swanson EA A, Lin CP P, et al. Optical coherence tomography. Science (80-) 1991:1178–81. Doi: 10.1126/science.1957169.

83 Fercher Adolf Friedrich, Drexler W, Hitzenberger CK, Lasser T. Optical coherence tomography – development, principles, applications. Z Med Phys 2010;20(4):251–76. Doi: http://dx.doi.org/10.1016/j.zemedi.2009.11.002.

84 Lee Sang-Hee, Lee Jong-Jin, Chung Hyun-Jin, Park Jong-Tae, Kim Hee-Jin. Dental optical coherence tomography: new potential diagnostic system for cracked-tooth syndrome. Surg Radiol Anat 2016;38(1):49–54. Doi: 10.1007/s00276-015-1514-8.

85 Youssefzadeh Soraya, Gahleitner André, Dorffner Roland, Bernhart Thomas, Kainberger Franz M. Dental Vertical Root Fractures: Value of CT in Detection. Radiology 1999;210(2):545–9. Doi: 10.1148/radiology.210.2.r99ja20545.

86 Idiyatullin Djaudat, Garwood Michael, Gaalaas Laurence, Nixdorf Donald R. Role of MRI for detecting micro cracks in teeth. Dentomaxillofacial Radiol 2016;45(7). Doi: 10.1259/dmfr.20160150.

87 Garwood Michael, Idiyatullin Djaudat, Corum Curtis A, et al. Capturing Signals from Fast-relaxing Spins with Frequency-Swept MRI: SWIFT. Encycl Magn

Reson 2012. Doi: 10.1002/9780470034590.emrstm1259.

88 Idiyatullin Djaudat, Corum Curt, Moeller Steen, Prasad Hari S. NIH Public Access 2012;37(6):745–52. Doi: 10.1016/j.joen.2011.02.022.Dental.

89 Idiyatullin Djaudat, Corum Curtis A, Nixdorf Donald R, Garwood Michael. Intraoral approach for imaging teeth using the transverse B1 field components of an occlusally oriented loop coil. Magn Reson Med 2014;72(1):160–5. Doi: 10.1002/mrm.24893.

90 Tamse A, Fuss Z, Lustig J, Kaplavi J. An Evaluation of Endodontically Treated Vertically Fractured Teeth. J Endod 1999;25(7):506–8. Doi: 10.1016/S0099-2399(99)80292-1.

91 Nielsen R Blake, Alyassin Abdalmajeid M, Peters Donald D, Carnes David L, Lancaster Jack. Microcomputed tomography: An advanced system for detailed endodontic research. J Endod 1995;21(11):561–8. Doi: 10.1016/S0099-2399(06)80986-6.

92 UMN CMRR. SWIFT software n.d.

93 Hassan Bassam, Metska Maria Elissavet, Ozok Ahmet Rifat, van der Stelt Paul, Wesselink Paul Rudolf. Comparison of Five Cone Beam Computed Tomography Systems for the Detection of Vertical Root Fractures. J Endod 2010;36(1):126–9. Doi: 10.1016/j.joen.2009.09.013.

94 Landis J Richard, Koch Gary G. The Measurement of Observer Agreement for Categorical Data. Biometrics 1977;33(1):159. Doi: 10.2307/2529310.

95 Sim Julius, Wright Chris C. The Kappa Statistic in Reliability Studies: Use, Interpretation, and Sample Size Requirements. Phys Ther 2005;85(3):257–68. Doi: 10.1016/s0161-4754(99)70126-0.

96 Dworkin SF, LeResche L. Research diagnostic criteria for temporomandibular disorders: review, criteria, examinations and specifications, critique. J Craniomandib Disord 1992;6(4):301–55.

97 Flahault Antoine, Cadilhac Michel, Thomas Guy. Sample size calculation should be performed for design accuracy in diagnostic test studies. J Clin Epidemiol 2005;58(8):859–62. Doi: 10.1016/j.jclinepi.2004.12.009.

98 Hassan Bassam, Metska Maria Elissavet, Ozok Ahmet Rifat, van der Stelt Paul, Wesselink Paul Rudolf. Detection of Vertical Root Fractures in Endodontically Treated Teeth by a Cone Beam Computed Tomography Scan. J Endod 2009;35(5):719–22. Doi: 10.1016/j.joen.2009.01.022.

99 Weishaupt Dominik, Köchli Victor D, Marincek Borut. *How does MRI work?*. 2008.

100 Walton Richard E, Michelich Robert J, Smith G Norman. The histopathogenesis of vertical root fractures. J Endod 1984;10(2):48–56. Doi: 10.1016/S0099-2399(84)80037-0.

101 Patel S, Dawood A, Pitt Ford T, Whaites E. The potential applications of cone beam computed tomography in the management of endodontic problems. Int Endod J 2007;40(10):818–30. Doi: 10.1111/j.1365-2591.2007.01299.x.

102 Shinozima Masayasu, Kohirazawa Hideo, Kubota Kazuro, Tokui Mitsuru. Tomorex (curved rotational tomography apparatus) in experimental and clinical practice. Oral Surgery, Oral Med Oral Pathol 1982;53(1):94–110. Doi: 10.1016/0030-4220(82)90493-5.

103 Jacobson Arnold F, Ferguson John P. Evaluation of an S. S. White Panorex x-ray machine. Oral Surgery, Oral Med Oral Pathol 1973;36(3):426–42. Doi: 10.1016/0030-4220(73)90223-5.

104 Lund TM, Manson-Hing LR. Relations between tooth positions and focal troughs of panoramic machines. Oral Surgery, Oral Med Oral Pathol 1975;40(2):285–93. Doi: 10.1016/0030-4220(75)90162-0.

105 Fornell Dave. Mayo Clinic Unveils Prototype of Smaller MRI Scanner. Imaging Technol News 2016.

106 Scarfe William C, Farman Allan G. What is Cone-Beam CT and How Does it Work? Dent Clin North Am 2008;52(4):707–30. Doi: 10.1016/j.cden.2008.05.005.

Appendix I

Criteria for CBCT Crack/Fracture Presentation

Existing criteria from previous studies from Youssefzadeh et al 1999 (85) and Hassan et al 2009 (98) regarding the detection of vertical root fractures by CBCT and CT were utilized and adapted to closely mirror the terminology stated in the previously agreed upon criteria for MRI crack presentation presented earlier in this study.

1. A separation of the adjacent root segments on multiple contiguous image slices without the continuation of the hypo-attenuated line into the adjacent tissue (or water as was present in this *ex vivo* study design). This hypo-attenuated line must be observed within the confines of tooth structure, delineated by:
    a. *External tooth surface:* bounded by enamel, the external surface of dentin, or cemental tissue depending on the level of axial slice.
    b. *Internal tooth surface:* external extent of the pulpal cavity

For purposes of this study, the physical discontinuity must have the following criteria to be given a designation of a crack/fracture.

1. Hypo-attenuated line(s) must extend from the external boundary of the tooth to the pulpal cavity (or vice versa)* on multiple contiguous image slices.^
2. The overall contour of the external tooth surface and pulpal cavity must be maintained.**

Explanation of stated criteria:

*A. *These cracks are thought to be clinically significant.*
B. ^The criteria of multiple image slices allow for detection of an angled crack.
*C. **To prevent gross root discontinuities from mistakenly being classified as a crack.*

Furthermore, it is important to differentiate cracks/fractures from other commonly encountered pathologic changes in tooth morphology that may be observed in CBCT, and to rule out artifact and possible false positive identification. The following entities should be differentiated from cracks/fractures:

- Cases with metallic restorations or root fillings that usually exhibit multiple streak artifacts that traversed the root and adjacent tissue.
- Aberrations in dental anatomy or morphology which may include
    - Accessory, lateral or secondary pulp canal(s)
    - Canal ramifications
- Physiologic or pathologic processes which may include
    - Root Resorption (Inflammatory, Replacement, Surface, Cervical, External, Internal)
    - Caries

Appendix II

Training and Calibration Exercise Instructions

1. Please review the criteria for MRI and CBCT crack/fracture presentation documents prior to starting the image review (see attached documents in digital folder).
    - You are encouraged to reference these documents while reviewing the images.

2. Items to keep in mind for the study:
    - ***The images have been pre-cropped/edited to include the entire root segment (CEJ to apex).***
        i. Interpret ALL the available slices in each DICOM image file – i.e. the whole visible image as you see it, then make the determination if the image appearance is consistent with crack / fracture.
    - ***For each image:***
        i. *Note the single slice # that allows best visualization of the crack/fracture* – then draw this representation in a crude drawing of what you see on the screen
        ii. *Note the crack slice range #s of where the best visualized crack/fracture starts and stops.*
        iii. OPTIONAL Free Response: note any questions, concerns, artifact observed, etc. When possible, give the slice # as a reference
    - ***Fatigue:***
        i. Observers will self-determine their level of fatigue throughout the study. If you feel fatigued, please take a break at any time. Do not continue when fatigued.
        ii. General Guidelines:
            1. *When possible, image review periods should not exceed 60 continuous minutes without a break.*
            2. A suggested break would be 1hr time lapse between image review sessions
            3. Take as much time as needed, there are no time limits.
    - ***Questions:***
        i. Assistance or clarification can be requested at any time.

Appendix III

Instructions for Opening and Viewing MRI and CBCT Images

Location – 7th Floor Radiology Clinic, Moos Tower 7-234
Each of the 8 computer works stations should have all necessary software preloaded

1st – Locate and open the DICOM software and Experimental Study Image Files:

1. Locate and open the RadiAnt DICOM Viewer 64-bit program (denoted by "R A" green and white square logo as seen on the right)
    - IMPORTANT – each station has dual monitors, use the LEFT monitor for image viewing. The right monitor can be used for file management.

2. Locate the desktop folder titled: "Experimental Study Images"
    - Images #s 1 - 140 should be displayed.
    - Click to select the desired image number you would like to review.
    - Once selected, simply drag and drop anywhere into the RadiAnt program window you have running on your desktop. The selected image should now be open and ready for manipulation and interpretation.
    - Each successive image can simply be dragged and dropped into the RadiAnt program window. It will automatically overlay over your past image; therefore you do not need to close a previous image file to view a new one.

2nd – Once the file is open in the RadiAnt DICOM viewer, the image can be manipulated via basic software commands and controls as follows.

RadiAnt DICOM Viewer (64-bit) Tutorial

- OVERVIEW: Basic RadiAnt User Controls Review
    - http://www.radiantviewer.com/dicom-viewer-manual/

- Turning Image Notations Off:
    - Turn off by selecting the "A" in the menu screen, this will provide the image only to minimize distraction while reviewing.

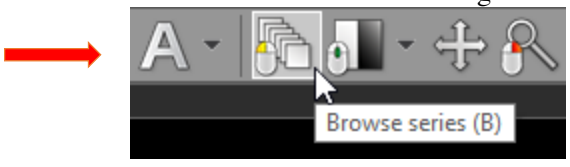

- "Full Dynamic Window": Using the preset image contrast auto-enhance
    - Image contrast can be auto-enhanced by using the preset "Full Dynamic Window" setting (pixel with the lowest value is displayed as black, whereas pixel with the highest value is displayed as white).

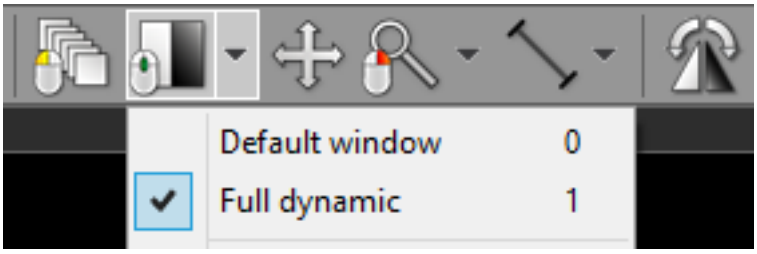

- NOTE: For best use of this feature, first browse the image (see instructions below) to a slice that shows visible tooth structure, usually moving the scroll bar ¾ of the way down works, THEN select “Full Dynamic Window” to auto-enhance the contrast. Brightness and contrast can be continually changed to the observer’s preference even after applying the “Full Dynamic Window” preset.
- If the tooth structure is not observed on any slice: proceed to pick a slice near the middle of the stack and next change the brightness and contrast (instructions below) to allow visualization of the tooth. In some instances the contrast may have to be lowered substantially to view the tooth. After visualization of tooth, THEN select “Full Dynamic Window” to auto-enhance. Brightness and contrast can be continually changed to the observer’s preference even after applying the “Full Dynamic Window” preset.

- Browsing Images:

There are several different ways of paging through the images of the series:

Click the Browse series button on the toolbar (or press the B key). Next, press the left mouse button over the image, and drag the mouse up or down to browse a series in both directions.

Turn the mouse wheel while the cursor hovers over the panel with the image.
Use the scrollbar on the right side of the panel.
Press the Up Arrow or Down Arrow on the keyboard to return to the previous image, or move on to the next.
Press Page Up or Page Down to move 10 images backward or forward.

- 6. On a multi-touch device, touch the image with one finger and drag it up or down. (The tool must be associated with the left mouse button - if it is not, touch the "Browse series" tool button.)

- Changing Brightness and Contrast:

Click the Adjust image window button on the toolbar (or press the W key).

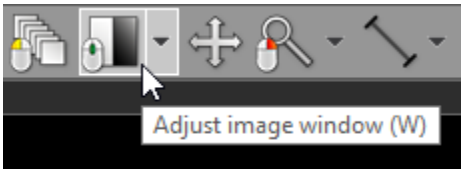

Next, press the left mouse button over the image and drag the mouse to change brightness (window level - WL), or contrast (window width - WW):

•Up to decrease brightness (window level goes up)
•Down to increase brightness (window level goes down)

•Left to increase contrast (window width shrinks)
•Right to decrease contrast (window width expands)

- Image Zooming

Click the Zoom image button on the toolbar (or press the Z key).

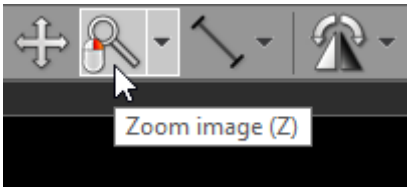

Next, press left mouse button over the image and drag the mouse Up to zoom in or Down to zoom out.

  - By default, the zooming tool is associated with the right mouse button.

- Image Panning

When an image is zoomed in, panning can be used to reveal areas lying outside the viewing panel.
Click the Pan image button on the toolbar (or press the M key).

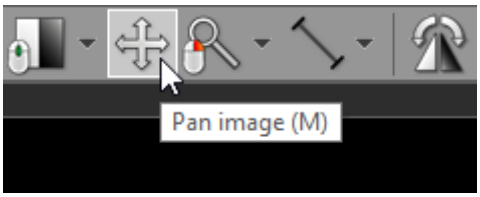

Next, press the left mouse button over the image and drag the mouse to move image around the screen.

Appendix IV

Observer Data Collection Form			Name:
Image Sample	Crack/Fx Detection	Location of Crack(s)/Fracture(s)	Specific Image Comments (**Optional**)
Image #	Is the Image Appearance Consistent with a Crack/Fracture? ("Y" or "N")	1. Note the SINGLE Slice # that Allows Best Visualization 2. As Seen on Screen, Draw the Cross-Sectional Outline of the Root(s) and the Location(s) of the Crack(s)/Fracture(s) with Line(s) 3. Note the Slice Range # That Contains the Crack(s)/Fracture	*Free Response:* Questions, Concerns, Artifact Observed, Etc. (Give Slice # as Reference if Possible)
1		Best Single Slice #: Drawing: Crack/Fx Slice Range #:	
2		Best Single Slice #: Drawing: Crack Slice Range #:	
3		Best Single Slice #: Drawing: Crack Slice Range #:	
4		Best Single Slice #: Drawing: Crack Slice Range #:	

Appendix V – Raw Study Data

Appendix VI

Key for Interpreting Raw Study Data (*in Appendix VII*)

CT A1	CT Imaging, Observer A, 1st Test
CT A2	CT Imaging, Observer A, 2nd Test (i.e. Re-Test - 20% were randomly re-tested)
CT B1	CT Imaging, Observer B, 1st Test
CT B2	CT Imaging, Observer B, 2nd Test (i.e. Re-Test - 20% were randomly re-tested)
CT C1	CT Imaging, Observer C, 1st Test
CT C2	CT Imaging, Observer C, 2nd Test (i.e. Re-Test - 20% were randomly re-tested)
CT D1	CT Imaging, Observer D, 1st Test
CT D2	CT Imaging, Observer D, 2nd Test (i.e. Re-Test - 20% were randomly re-tested)
MRI A1	MR Imaging, Observer A, 1st Test
MRI A2	MR Imaging, Observer A, 2nd Test (i.e. Re-Test - 20% were randomly re-tested)
MRI B1	MR Imaging, Observer B, 1st Test
MRI B2	MR Imaging, Observer B, 2nd Test (i.e. Re-Test - 20% were randomly re-tested)
MRI C1	MR Imaging, Observer C, 1st Test
MRI C2	MR Imaging, Observer C, 2nd Test (i.e. Re-Test - 20% were randomly re-tested)
MRI D1	MR Imaging, Observer D, 1st Test
MRI D2	MR Imaging, Observer D, 2nd Test (i.e. Re-Test - 20% were randomly re-tested)

Appendix VII

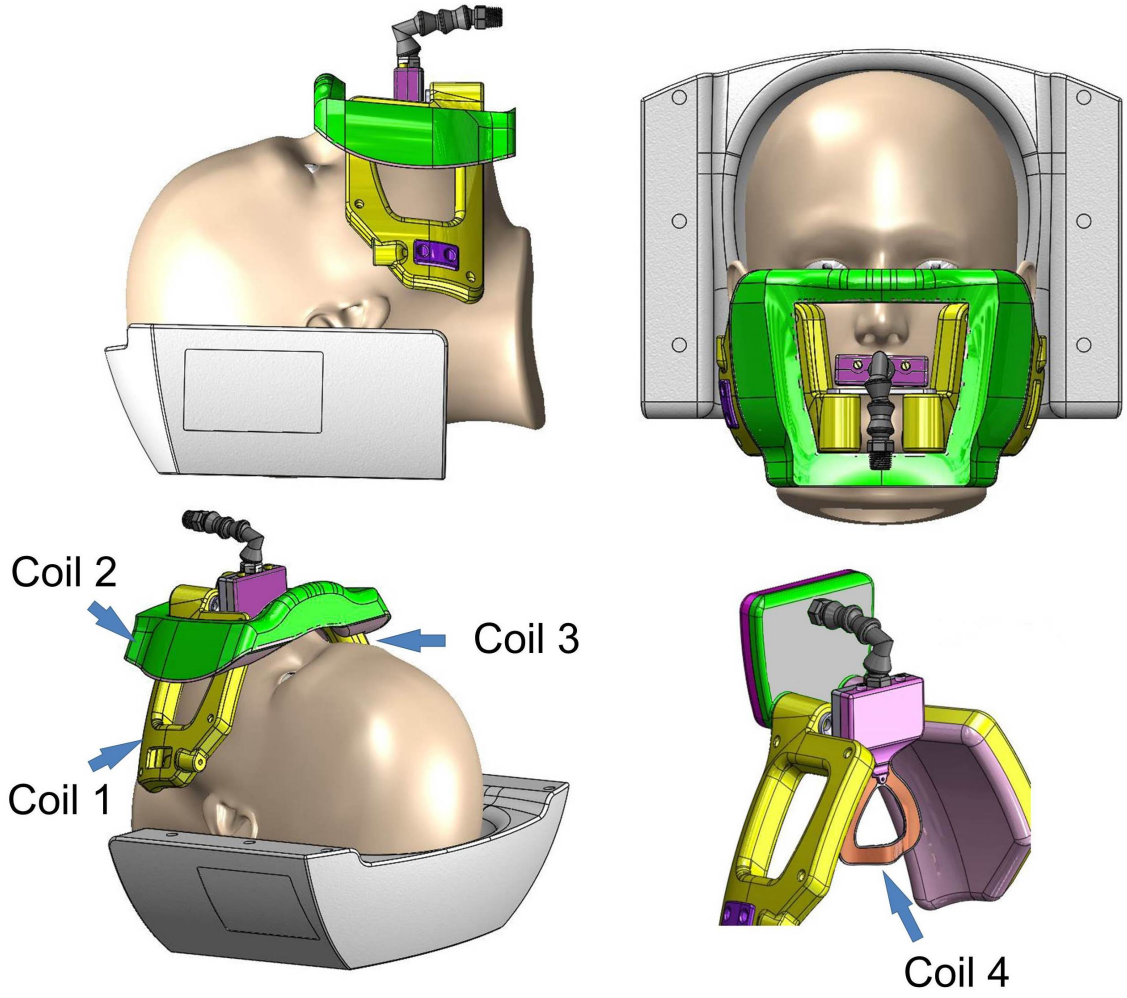

Figure 21. Newly-designed, custom-built, intra-oral/extra-oral coil developed at UMN's CMRR following completion of the experimental phase; this coil was not utilized in the current study, but will be utilized in future studies (coil design and figure courtesy of [DI]).